CHAPTER 5

Non-Volcanic Stratospheric Aerosol Trends: 1971 – 2004

Lead Authors:
Terry Deshler
Richard Anderson-Sprecher

Authors:
John Barnes
Barclay Clemesha
Sophie Godin-Beekmann
Roy Grainger
David Hofmann
Horst Jäger
Steven Marsh
Mary Osborn
Dale Simonich

5.1   Introduction

The existence of persistent atmospheric aerosol after volcanic eruptions must have been apparent to careful observers from early times. The reddish diffraction ring around the sun following large volcanic eruptions was first described by Sereno Bishop nine days after the eruption of Krakatoa, in late August 1883, and led to the name Bishop's ring. Less certain is that early observers suspected that aerosol persisted in the stratosphere during volcanically quiescent periods. The first published report suggesting a persistent aerosol layer in the stratosphere used purple twilight observations [Gruner and Kleinert, 1927]. Quantitative observations characterizing the altitudes, sizes, masses, and aerosol compositions involved were first provided by balloonborne impactor measurements in the late 1950s [Junge et al., 1961]. Subsequent measurements by both aircraft- and balloon-borne impactors suggested the global distribution of stratospheric aerosol [Junge and Manson, 1961; Chagnon and Junge, 1961]. On a few occasions, in addition to the impactors which measured particles > 0.1 μm, Aitken particle counters were included on the balloon gondola. While the Aitken nuclei concentration decreased through the stratosphere, particles > 0.1 μm had a maximum in concentration near 20 km, suggesting an aerosol source in this region [Junge et al., 1961]. These particles were large enough to create the purple twilight noted by early observers; however, recent work suggests that tropospheric aerosol must also contribute to the purple twilight in cases of a clean stratosphere [Lee and Hernandez-Andres, 2003].

Junge et al.'s measurements were at the end of an extended volcanic-free period [Stothers, 1996], but did not establish a baseline for stratospheric aerosol. Quantifying the global stratospheric aerosol burden, and describing the role of volcanic eruptions, required long term measurements which began in the early 1970s using balloonborne particle counters [Hofmann et al., 1975; Hofmann and Rosen, 1980; Hofmann, 1990]; lidar [Jäger, 2005; Osborn et al., 1995; DeFoor et al., 1992]; and in the late 1970s satellite instruments: SAM (Stratospheric Aerosol Measurements) II (1979-1994) [Pepin et al., 1977; Poole and Pitts, 1994], SAGE (1979-1981) (Stratospheric Aerosol and Gas Experiment) and SAGE II (1984-present) [McCormick et al., 1979, Chu et al., 1989; Thomason et al., 1997]. The impact of sulfur rich volcanic eruptions then became obvious and these have been the dominant source of stratospheric aerosol for the past 30 years. Within the last century the most recent 30-year period has been a relatively active volcanic period. Sato et al. [1993] and Stothers [1996], using solar and stellar extinction data, show that the previous 120 years was dominated by eight major eruptions. Four of these occurred between 1880 and 1910 and four since 1960. The long term measurements which began in the 1970s, have captured the complete cycle for three major eruptions with a global stratospheric impact: Fuego (14°N, October 1974, 3-6 Tg of aerosol), El Chichón (17°N, April 1982, 12 Tg) and Pinatubo (15°N, June 1991, 30 Tg) [McCormick et al., 1995]. Within this record there have been four periods when volcanic influences were at a minimum, 1974, 1978-1980, 1988-1991, and 1997 - present. Table 5.1 summarizes the volcanic activity between 1960 and 2003, including eruptions with stratospheric importance, generally volcano explosivity index (VEI) $\geq$ 4 [Carn et al., 2003; Newhall and Self, 1982; Simkin and Siebert, 1994; the web pages of the Smithsonian Global Volcanism Network; Schnetzler et al., 1997; Halmer et al., 2002]. Also in Table 5.1 the SO_2 and aerosol loading, if available, are included. Most SO_2 estimates are from Total Ozone Mapping Spectrometer (TOMS) data [Carn et al., 2003]. Missing estimates primarily occur prior to TOMS measurements. Missing estimates since 1979 indicate that information for that volcano was not available.

Table 5.1. Names, locations, dates, Volcano Explosivity Index (VEI) and SO$_2$ and aerosol loading, when available, for all stratospherically important eruptions 1960 - 2003 [Carn et al., 2003; Simkin and Siebert, 1994; Smithsonian Global Volcanism Network, Schnetzler et al., 1997; Halmer et al., 2002].

Name	Lat	Long	Date	Year	VEI	Aerosol Loading	
						SO$_2$(Mt)	Aerosol (Tg)
Agung	8.3 S	115.. E	Mar 17	1963	5		16-30
			May 16		4		
Shiveluch	56.6 N	161.4 E	Nov 12	1964	4+		
Taal	14.0 N	121.0 E	Sept 28	1965	4		
Kelut	7.9 S	112.3 E	April 26	1966	4		
Awu	3.7 N	125.. E	Aug 12	1966	4		
Fernandino	0.4 S	91.5 W	June 11	1968	4		
Tiatia	44.3 N	146.3 E	Jul 14	1973	4		
Fuego	14.5 N	90.9 W	Oct 14-17	1974	4		3-6
Tobalchik	55.8 N	160.3 E	Jul 6	1975	4+		
Augustine	59.4 N	153.4 W	Jan 22	1976	4		
Soufriere	13.3 N	61.2 W	Apr 14, 17	1979	3		
Sierra Negra	0.8 S	91.2 W	Nov 13	1979	3		
Saint Helens	46.2 N	122.2 W	May 18	1980	5	1.0	
Ulawun	5.0 S	151.3 E	Oct 6 & 7	1980	3		
Alaid	50.9 N	155.6 E	Apr 27-30	1981	4	1.1	
Pagan	18.1 N	145.8 E	May 15	1981	4	0.3	
Nyamuragira	1.4 S	29.2 E	Dec 25	1981	3		
El Chichón	17.0 N	93.2 W	Mar 28	1982	4	8.1	12
			Apr 4		5		
Galunggung	7.3 S	108.0 E	May 17	1982	4		
Colo	0.17 S	121.6 E	Jul 23	1983	4	0.2	
Nevado del Ruiz	4.90 N	75.3 W	Nov 13	1985	3		
Augustine	59.4 N	153.4 W	Mar 27	1986	4?	<0.05	
Nyamuragira	1.4 S	29.2 E	Jul 16	1986	4	0.8	
Chikurachki	50.3 N	155.. E	Nov 20	1986	4?		
Kelut	7.9 S	112.3 E	Feb 10	1990	4	<0.05	
Pinatubo	15.0 N	120.3 E	June 12	1991	6(5+)	17-20	30
Cerro Hudson	45.9 S	73.0 W	Dec 8	1991	5+	3.3	3
Spurr	61.3 N	152.3 W	Jun 27	1992	4	0.2	
Lascar	23.4 S	67.7 W	Apr 19	1993	4	0.4	
Rabaul	4.3 S	152.2 E	Sep 19	1994	4?	0.2	
Kliuchevskoi	56.1 N	160.6 E	Oct 1	1994	4 (3?)	0.1	
Shishaldin	54.8 N	164.0 W	Apr 19	1999	3		
Ulawun	5.05 S	151.3 E	Sep 29	2000	4	<0.05	
Shiveluch	56.6 N	161.4 E	May 22	2001	4?	0	

The VEI, developed by Newhall and Self [1982] to characterize volcanoes, is indicative of the volume of ejecta and the height of the eruption column. The height ranges for a VEI of 3, 4, and 5 are 3-15 km, 10-25 km, and >25 km. VEI alone, however, cannot predict stratospheric impact. Only sulfur rich volcanic eruptions provide the sulfur necessary to form sulfuric acid which then condenses with water into tiny droplets which have stratospheric lifetimes of years. Thus VEI must be coupled with the amount of sulfur ejected from the volcano. For example, Mt. St. Helens, with a VEI of 5.0, contained little sulfur (< 1 Mt), thus the stratosphere was not greatly perturbed by Mt. St. Helens [Robock, 1981], and, if not for El Chichón, stratospheric aerosol would have returned to background within a few years of the

eruption. Schnetzler et al. [1997] and Halmer et al. [2002] have coupled VEI with sulfur emissions to produce a volcanic SO_2 index which is more indicative of the stratospheric impact of a volcano.

The primary emphasis of long term stratospheric aerosol measurements has been on volcanic events. This is partly due to the significant impact large eruptions have on the stratosphere, to the increased signal they provide for instruments, to the dynamic nature of eruptions and their aftermath, to their global distribution, and to the fact that volcanic eruptions have dominated the signal for 20 of the past 30 years [Barnes and Hofmann, 2001; Deshler et al., 2003; Jäger, 2005]. In addition these eruptions are important for analyzing short-term regional and global effects on climate from enhanced stratospheric aerosol loading [Hansen et al., 1992; Dutton and Christy, 1992]. This analysis is important for climate models. Aerosols play an important role in radiative processes, thus influencing the consequences of changing trace gas concentrations in the atmosphere, and altering photolysis rates and the concentrations of trace gases, e.g. ozone, in the atmosphere. The focus here, however, is on long-term non-volcanic variations of stratospheric aerosol levels. Thus the emphasis shall be on levels present during years between major eruptions, rather than on temporary enhancements due to volcanic eruptions. Stratospheric aerosol during non-volcanic periods is referred to as background aerosol. This background aerosol level will be subject to various periodic perturbations, such as seasonal cycles, and long-term secular changes that govern the overall trend in the record. Identifying secular trends in the background aerosol is crucial to predict future aerosol levels.

The background stratospheric aerosol level is defined as that level at which fluctuations in the aerosol loading can no longer be ascribed to specific volcanic injections. It is anticipated that natural and anthropogenic emissions of sulfur, in the form of OCS and SO_2, will then be sufficient to maintain a population of stratospheric aerosol in quasi-steady state. During background periods measurements are expected to remain within variations expected due to measurement error, measurement frequency, and non-volcanic geophysical oscillations, such as induced by season or the quasi-biennial oscillation (QBO). Although serious questions may be raised about the extent to which inter-volcanic periods over the past 30 years have reached background, measurements during these periods provide the only information available to compare stratospheric aerosol in background periods. The best that can be provided is an objective analysis of these measurements. A further complication results from primarily the use of instruments sensitive to bulk aerosol quantities, such as extinction or backscatter, for long term measurements. Thus fine scale changes in aerosol size distribution may be difficult to observe.

The importance of possible changes in background stratospheric aerosol levels led to the analysis of each quiescent period as it appeared in the record. The first of these analyses [Hofmann and Rosen, 1980; Hofmann and Rosen, 1981; Sedlacek et al., 1983] compared the pre-Fuego and pre-El Chichón periods. Comparison of pre-El Chichón measurements with initial measurements of Junge et al. [1961], which were at the end of an extensive volcanic-free period, suggested a possible increase of about a factor of five in aerosol concentration at 20 km during the intervening 20 years leading Hofmann and Rosen [1980] to suggest an increase of 9% yr^{-1} in aerosol mixing ratio for aerosol > 0.15 μm radius. Sedlacek et al. [1983], comparing globally distributed airborne filter samples during 1974 and 1979, pre-Fuego and pre-El Chichón, suggested a 6% yr^{-1} increase in background stratospheric sulfur mass. Figure 5.1 presents the long term aerosol measurements from Laramie, Wyoming, initiated by Hofmann et al. [1975], with Junge's initial measurements at nearly the same latitude [Chagnon and Junge, 1961]. Based on instrumental characteristics, Junge et al. [1961]

suggest that their measurements collected particles > 0.15 μm radius with a 55% efficiency. The integrals shown in Figure 5.1 account for this collection efficiency and assume the Wyoming measurements have a 100% collection efficiency, the case which would lead to the minimum difference between measurements, whereas the comparisons shown in Hofmann and Rosen [1980] assume the 55% collection efficiency applied to the Wyoming measurements as well. Applying a collection efficiency of 55% only to Junge et al.'s measurements would have reduced Hofmann and Rosen's [1980] estimate to 6 % yr^{-1}, instead of 9 % yr^{-1}. Comparing the average of Junge's measurements shown in Figure 5.1 with the minimum in column integrals observed in 1979 suggests a more conservative increase of 2% yr^{-1}, but as apparent from Figure 5.1, would have still suggested a significant increase in background aerosol.

During volcanically quiescent periods the sulfur for stratospheric aerosol arises from the transport of tropospheric OCS, SO_2, and sulfate aerosol into the stratosphere. The fractional contributions of OCS, SO_2, and sulfate aerosol to stratospheric aerosol are approximately 35, 25, and 40%, obtained by combining estimates from Weisenstein et al. [1997] and Pitari et al. [2002]. Between 1960 and 1980 anthropogenic emissions of SO_2 increased by over 2% yr^{-1}. Assuming that natural sources of SO_2 remained fairly constant at about 30% of total SO_2 emissions [Pitari et al., 2002], this implies an increase of ~1.6% yr^{-1} in SO_2 emissions between 1960 and 1980 [van Ardenne et al., 2001]. During this same period
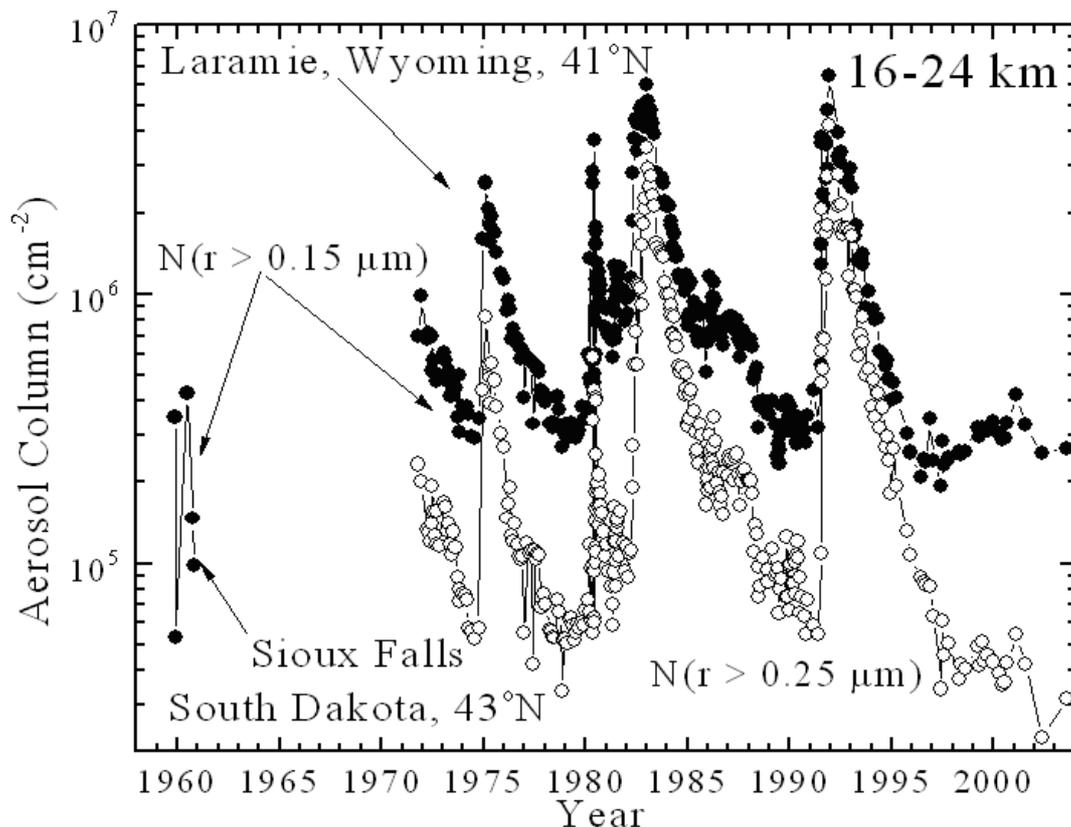

Figure 5.1. Aerosol columns, 16-24 km, for balloonborne in situ measurements of particles with radius > 0.15 μm (filled circles) above Sioux Falls (43°N), 1959-1960 [Chagnon and Junge, 1961], and above Laramie (41°N), 1971-2003. Also included in the Laramie measurements are particles with radius > 0.25 μm (open circles).

OCS increased at a rate of approximately 0.5% yr^{-1} [Montzka et al., 2004]. If these increases in SO_2 and OCS are weighted according to their fractional contribution to stratospheric aerosol, assuming that the contribution of sulfate aerosol remains constant, and that stratospheric aerosol responds linearly with respect to source gases, then the increase in stratospheric aerosol can be estimated. These estimates indicate an increase of ~0.6% yr^{-1}, well below Hoffman and Rosen's [1980] estimate of 9% yr^{-1} and even the more conservative estimate of 2% yr^{-1} indicated in Figure 5.1. A linear response to changes in source gases is consistent with sensitivity studies to changes in OCS performed with a 2-D model, see Weisenstein et al. [1997] and Chapter 6 of this report.

With the benefit of the present post Pinatubo Wyoming measurements of background aerosol, and considering the scatter in the initial measurements reported by Chagnon and Junge [1961], it appears that the initial measurements of Chagnon and Junge did not fully account for the sampling efficiency of the instrument, or the instrument was sensitive to particles somewhat larger than 0.15 μm, a possibility considered earlier [Hofmann and Rosen, 1981], but dismissed. In any case it is clear from Figure 5.1 why initial measurements in the 1970 and early 1980 background periods were interpreted as indicating an aerosol increase [Hofmann and Rosen, 1980; 1981]. The aerosol increase observed, however, exceeds what may have been expected based on changes in aerosol source gases.

The question of changes in background stratospheric aerosol was revisited prior to the Pinatubo eruption. Hofmann [1990] compared measurements of aerosol mixing ratio for 0.15 and 0.25 μm radius thresholds during volcanically unperturbed periods in 1974, 1979, and 1989. No change was observed in the mixing ratio of 0.15 μm particles; however, there was a 50% increase in aerosol mixing ratio for particles > 0.25 μm between 1979 and 1989. Based on this increase Hofmann estimated an increase in aerosol mass on the order of 5% yr^{-1} over the decade which is consistent with the earlier estimates of Hofmann and Rosen [1980] and Sedlacek et al. [1983]. A similar increase over the same time period was observed when SAGE I and II measurements were compared; however, Thomason et al. [1997] suggested that 1989 may not have been at true background level, due primarily to Nevado del Ruiz in 1985 and Nyamuragira in 1986. Thus they suggested the elevated aerosol was due to residual volcanic effects. OCS over this period increased by approximately 2% [Montzka et al., 2004] about half of the increase observed by Hofmann [1990].

Resolution of the questions raised by these studies had to wait for the third background period in the modern record, the present post Pinatubo period. Based on long term lidar measurements at Mauna Loa, Hawaii, Barnes and Hofmann [1997] suggest that the decay of aerosol loading following El Chichón and Pinatubo was influenced by the phase of the QBO in tropical stratospheric winds (also evident in the Garmisch lidar data, Jäger [2005]) and that integrated aerosol backscatter in 1995 was below any previous observation at Mauna Loa. Hayashida and Horikawa [2001] used SAGE II extinction measurements to derive Ångström parameters and concluded that the pre-Pinatubo period was still influenced by volcanic eruptions from the mid 1980s and cannot be considered a real background period. Barnes and Hofmann [2001] used the present background period, extending from 1996, to demonstrate variability correlated with the phase of the QBO, with implications for the source of background stratospheric aerosol. Thirty year records of in situ [Deshler et al., 2003] and remote [Jäger, 2005] mid-latitude measurements suggest that stratospheric aerosol in the present, post-Pinatubo period is at or below any previous background period since 1970. These analyses of the post-Pinatubo aerosol suggest, in contrast to studies of earlier background periods, no long term increase in stratospheric background aerosol.

The purpose here is to examine all long term stratospheric aerosol measurements for trends in the background aerosol. This requires records which span at least two of the four volcanically quiescent periods in the modern aerosol record, limiting the data set to the six longest stratospheric aerosol measurement records available. These are: 1) in situ aerosol concentration measurements at 0.15 and 0.25 µm radius from Laramie, Wyoming, USA (1971-2003, 41°N); remote lidar backscatter measurements from: 2) São José dos Campos, Brazil (1972-2003, 23°S), 3) Mauna Loa, Hawaii, USA (1974-2003, 20°N), 4) Hampton, Virginia, USA (1974-2002, 37°N), 5) Garmisch-Partenkirchen, Germany (1976-2002, 48°N); and 6) remote satellite extinction measurements from SAM II (1979-1994), SAGE I (1979-1981) and SAGE II (1984-2003). For each of these measurement platforms the fundamental measurements will be described and then compared during the volcanically quiescent periods, taking into account instrumental or operational changes in the measurements.

5.2   Fundamental measurements

5.2.1   In situ measurements

Stratospheric aerosol measurements at Laramie, Wyoming, began in 1971 using an optical particle counter (OPC) initially developed by Rosen [1964]. The instrument measures the intensity of scattered white light at 25° in the forward direction from single particles passing through the light beam which is larger than the air sample stream. Mie theory is used to determine aerosol size from the amount of scattered light. Initial measurements in the 1970s consisted of measurements of the concentration of particles with radius $\geq$ 0.15 and 0.25 µm at a sample flow rate of 1 liter min^{-1} [Pinnick and Hofmann, 1973; Hofmann et al., 1975]. In 1989, the OPC was modified to make measurements for particles > 0.4 µm, to increase the number of sizes measured, and to decrease the minimum concentration measurable [Hofmann and Deshler, 1991]. The scattering angle of the detector axis was increased from 25 to 40° and the air sample flow rate increased from 1 to 10 liters min^{-1}, with appropriate changes in inlet design to maintain roughly isokinetic sampling. This new scattering angle allowed unambiguous detection of particles throughout the size range 0.15 - 10.0 µm. After calibration flights in Laramie to insure that the measurements at 0.15 and 0.25 µm radius are, within measurement limits, the same for counters with scattering angles at 25 and 40°, the new OPC replaced the old OPC for regular flights in Laramie beginning in 1991 [Deshler et al., 1993; Deshler et al., 2003].

A more complete description of the instrument and discussion of error sources is provided in Deshler et al. [2003] and in Chapter 3. Here the primary error sources are summarized. Sizing errors are 10% at 0.15 and 0.25 µm and result primarily from pulse broadening by photo multiplier tubes. Errors in concentrations are controlled by Poisson counting statistics or a precision of $\pm$ 10% when Poisson counting statistics are not a factor. Poisson uncertainties lead to concentration uncertainties of 85, 25, and 8% for concentrations of 0.01, 0.1, and 1.0 cm^{-3} at a sample rate of 1.0 liter min^{-1} and concentrations of 0.001, 0.01, 0.1 cm^{-3} at 10 liters min^{-1}.

5.2.2   Remote lidar measurements

The first lidar (light detection and ranging) measurements of stratospheric aerosol were completed shortly after Junge et al.'s initial measurements [Fiocco and Grams, 1964]. Lidars provide remote, vertically resolved measurements of atmospheric backscatter at one or more wavelengths. Lidar sites investigating stratospheric aerosols now range in latitude from 90°S

to 80°N, with a number of sites in northern mid latitudes, and a few stations in the sub tropics and southern mid latitudes. The standard measurement from any lidar is backscatter which is the fraction of incident light intensity returned at 180° to the incident light pulse. The backscatter is presented as fraction per steradian per meter of scattering medium. Atmospheric backscatter arises from both molecular (Rayleigh) and aerosol (Mie) scattering. Backscatter also arises from non-spherical particles which do not follow Mie theory (e.g. ice particles, or fresh volcanic ash particles). To obtain aerosol profiles from a lidar requires accounting for three factors which affect the backscattered light received by the lidar telescope: 1) two way light extinction, 2) molecular backscatter, and 3) instrument normalization [e.g. Russell and Hake, 1977]. Molecular backscatter and extinction is typically calculated from pressure/temperature profiles provided by a nearby radiosonde station. In an aerosol free atmosphere, and with a perfectly calibrated lidar, molecular backscatter would coincide with the lidar backscattering measured.

Uncertainties in lidar measurements arise from two-way extinction of the lidar signal, the difficulty of determining an aerosol free region for normalization, signal induced noise, and from detector non-linearity for analog detection systems, or pulse overlapping for photon counting systems. For volcanic conditions there is a large aerosol signal, well above the molecular signal, resulting in small uncertainties. For quiescent conditions aerosol backscatter is less than 5% of molecular scattering, requiring longer integration times. The two-way particle extinction of the lidar signal becomes significant during periods of high aerosol loading but is reduced considerably for measurements during background periods [Simonich and Clemesha, 1989]. The purely instrumental errors from effects such as signal-induced noise can be reduced significantly by careful instrumental design. Long-term calibration problems do not arise because, for each measurement, aerosol back-scatter is determined only after the lidar signal is forced to match that expected from a purely molecular atmosphere at the altitude of normalization. The main source of error is in uncertainties in the molecular profile corresponding to a given lidar profile. The sources of molecular profiles and the estimated precision are given below for each of the lidar series used in this study.

The four lidar records included here are the only multi-decadal lidar records available. They are based at São José dos Campos, Brazil (23.2°S, 45.9°W), Mauna Loa, Hawaii (19.5°N, 155.6°W), Hampton, Virginia (37.1°N, 76.3°W), and Garmisch-Partenkirchen, Germany (47.5°N, 11.1°E). To reduce variations in the measurements due to variations in altitude and thickness of the aerosol layer, the quantity used for long time series comparisons is the vertically integrated backscatter coefficient with units of sr^{-1}. Each lidar will be compared to its own record to assess changes during background periods, but for interest the two tropical/sub tropical and mid latitude lidars are also compared to each other.

 The São José dos Campos measurements use the sodium D_2 line at 589 nm and began in 1972. The primary focus of these measurements has been on the atmospheric sodium layer; however, measurements of the stratospheric aerosol content are also available (Clemesha and Simonich, 1978; Simonich and Clemesha, 1997). The wavelength used for the measurements has not changed during the period, although there have been major changes in the laser and improvements in the electronics. Since this site is in the sub tropics, tropopause height fluctuations and variations in the atmospheric density profile are minor. The molecular density profile used is an annual average derived from rawinsonde measurements. An iterative procedure is used to account for aerosol extinction. Ozone absorption is negligible. The measurements presented here represent monthly averages of integrated aerosol backscatter from 17 to 35 km. Error estimates on the integrated profiles are ±5%. The number of

measurements per month is dependent on season, more in winter, but averages about 3.7 days per month.

The Mauna Loa, Hawaii, measurements, using a ruby laser, 694 nm, began in 1974 with the main focus on stratospheric aerosol [DeFoor et al., 1992; Barnes and Hofmann, 1997; 2001]. In 1994 a new lidar was built using a Nd:YAG laser measuring backscatter at both the 532-nm harmonic and the 1064-nm fundamental. For data continuity, the 532-nm measurements are converted to 694 nm for easy comparison with the early measurements. There was an overlapping period of about a year (40 observations) during which the ruby lidar backscatter and the Nd:YAG lidar backscatter at both wavelengths were measured. The average absolute backscatter of the ruby lidar agreed to within 2% of the Nd:YAG backscatter interpolated to 694 nm from the measurements at 532 and 1064 nm. The conversion factor obtained from the interpolation is used for the entire 532 nm data set. Errors on the integrated backscatter range from ±15 to > ±30% for the ruby measurements, depending on aerosol load. These errors are reduced to approximately ±6% for the 532-nm measurements. Since this is another tropical station tropopause fluctuations are minor and the altitude interval for backscatter calculation can be fixed. In this case it is 15.8 to 33 km. Molecular density is obtained from a model for the Ruby lidar analysis and from the nearest radiosonde site (Hilo, Hawaii) for the Nd:YAG lidar.

The Hampton, Virginia, measurements also use a ruby laser, began in 1974, and are focused on stratospheric aerosol [Fuller et al., 1988; Woods et al., 1994; Osborn et al., 1995]. Although there have been incremental improvements in the system, the fundamental operating wavelength and measurement principles have not changed. For this mid latitude station the integration interval is from the tropopause to 30 km. Errors range from 15 - 50% during stratospheric background periods reducing to 5% for measurements following large eruptions. Molecular densities are obtained from a radiosonde station 120 km to the northeast.

The Garmisch-Partenkirchen, Germany, measurements began in 1976 with a ruby laser and are also focused on stratospheric aerosol [Reiter et al., 1979; Jäger, 2005]. There was an interruption in the measurements from May 1990 to March 1991 to convert the lidar to a Nd:YAG system. Measurements beginning in 1991 use the 532-nm harmonic of the Nd:YAG laser, and there was no overlap of the two lidars. As in the case of Mauna Loa, all 532-nm measurements are converted to 694 nm to easily compare with the earlier measurements. The conversion is based on height and time resolved wavelength dependencies which are calculated from particle size distributions applying Mie calculations [Jäger and Deshler, 2002 and 2003]. The size distribution data are derived from monthly measurements with balloonborne optical particle counters at Laramie, Wyoming [Deshler et al., 1993, 2003]. Backscatter integrations cover the altitude range, tropopause + 1 km to profile top. Error estimates range from 10 to 50%, depending on stratospheric aerosol load, for the ruby measurements. These errors are reduced by about half for the 532-nm measurements. Molecular density is obtained from a radiosonde station at Munich, 100 km to the north. Iteration is used to account for aerosol extinction.

5.2.3   Remote satellite measurements

The first satellite based aerosol measurement was completed in 1975 using a photometer pointed at the sun by the astronaut as the earth's limb passed in front of the sun [Pepin et al., 1977]. This led to the first regular satellite measurements of stratospheric aerosol using a single wavelength photometer measuring solar extinction during 15 sunrises and sunsets by the satellite per day, SAM II [McCormick et al., 1979; 1981; Russell et al., 1981]. The

multiwavelength SAGE and SAGE II instruments [Mauldin et al., 1985] followed close behind. These instruments are self calibrating since prior to or after each solar occultation the photometer measures the direct solar transmission without atmospheric extinction. Thus the measured extinction through the atmosphere is truly relative to the exo-atmospheric solar transmission with all instrument artifacts removed.

SAGE II measures solar transmission through the atmosphere with a spectral radiometer. To convert this to aerosol extinction the influence of gas molecules along the tangent line of sight must be removed, as well as gas and aerosol extinction from altitudes above the measurement altitude. The extinction at upper altitudes influences a measurement at the leading and tailing boundaries along the line of sight due to the spherical geometry. Removing these contributions is known as the onion peeling method. The inversion of the SAGE II solar occultation measurements to provide aerosol extinction is described by [Chu et al., 1989]. The effect of subtle changes in the SAGE II instrument are carefully monitored and are routinely evaluated for impact on data products including ozone and aerosol extinction [Thomason and Burton, 2005]. The 1020-nm aerosol extinction exhibits extremely limited sensitivity to changes in instrument characteristics like unobscured solar intensity measurements, dark current, and mirror reflectivity. The 525-nm aerosol channel is slightly more sensitive to such changes, but even there, the possible drift over the lifetime of the instrument is < 1%. Since SAGE II uses National Center for Environmental Protection (NCEP) estimates of molecular density for the computation of the molecular contribution to the line-of-sight transmission, a long-term drift between NCEP temperatures and the real atmosphere could introduce a drift of a few percent over the lifetime of the instrument, There has been a number of SAGE II validation and comparison efforts [Russell et al., 1984; Osborn et al., 1989; Oberbeck et al., 1989; Russell and McCormick, 1989; Hervig and Deshler, 2002]. As the understanding of the instrument performance has evolved a number of revisions of the SAGE II data have been provided; however, for our purposes the revisions are not critical. For any one revision the same data inversion is applied to all past measurements, thus the relative values of extinction over a 20 year period will stay the same even though the absolute values may change from one revision to another.

Of the eleven instruments deployed on satellites in the past 30 years which include stratospheric aerosol measurements, only SAGE II has a record long enough to consider for our purposes. This record can be extended somewhat by SAGE I. SAM II measurements span 12 years, 1979-1991, at high latitudes, 72-83° N/S [Poole and Pitts, 1994]. Although SAM II measurements are not strongly affected by volcanic eruptions, they have a strong annual cycle and wintertime measurements are influenced by polar stratospheric clouds. This coupled with the relatively short record limited our interest in SAM II to a simple inspection of the measurements, which does not show any clear temporal tendency. Only the SAGE II record was considered of sufficient length to be evaluated for trends.

5.3   Measurements

For the quantitative comparison of volcanically quiescent periods, the primary measurement from each instrument will be used. The measurements have been checked to be cloud and tropospheric aerosol free and are at latitudes ≤ 50°, thus will not be perturbed by polar stratospheric clouds. The screening is done using the local tropopause at each sampling site to determine the base of measurements to be included and relying on individual lidar and in situ investigators to insure no anomalous stratospheric cirrus are included. In fact these are extremely rare. For SAGE II the data selected for analysis were limited to measurements 2 km

above the SAGE II calculated tropopause, and the SAGE II extinctions were checked spectrally for clouds.

For the in situ measurements approximately monthly profiles of aerosol concentration for particles $\geq$ 0.15, 0.25 μm are integrated over altitude columns varying from 5 to 15 km. Typical tropopause heights at Laramie are 10-12 km extending to 15 km in the summer. Column integrals from 15-20 and 20-25 km are presented in Figure 5.2. Global SO_2 emissions since 1970 are shown in Figure 5.2b, the 1970-1990 estimates are from van Ardenne et al. [2001], while the 2000 SO_2 emissions are estimated based on extrapolating the 1990 estimate with a -2% yr^{-1} trend [Hicks et al., 2002]. Model estimates of aerosol during background periods for one year are also shown in Figure 5.2. Each model estimate, covering one year, is shown between 2001 and 2003. The model results are from one 3-D [Timmreck, 2001] and one 2-D [Weisenstein et al., 1997] model. The models, described in detail in Chapter 6, calculate aerosol particle densities in 35 or more bins from 0.001 to 2.58 μm as functions of latitude, altitude, and season. For the 20-25 km integral the two model estimates are ~50% above the measurements. The two models disagree on the 0.25 μm size. For 15-20 km both models agree, but overestimate the in situ concentration measurements by a factor of 3.

In Figure 5.2, the 0.15 μm column integrals reach a plateau between 1.5 and 2.0 x 10^5 cm^{-2} at both altitude intervals for the three background periods, while the 0.25 μm measurements show a bit more variation, remaining elevated in 1990 - 1991 compared to 1979 and 1997, particularly between 15 and 20 km. The 0.25 μm observations prior to Pinatubo were the reason for Hofmann's [1990] estimate of a 5% yr^{-1} increase in sulfur mass between 1979 and 1989.

The final measurements in 2002 and 2003 show striking variations, but suffer from a sampling frequency reduced to once per year. The particularly low measurement in 2002, 20-25 km, was checked carefully and was confirmed by two independent simultaneous measurements at 0.25 μm. Thirty day isentropic back trajectories at 570 and 690 K (~24 and 27 km) do not provide any useful insight. At 570 K the air passed through high latitudes, circulated in the central Pacific for ~10 days, and then moved eastward, nearly zonally, to Wyoming. At 690 K, the air meandered in the central Pacific, passed zonally to western Kansas, and then, in the final 10 days, circulated anticyclonically southward to New Mexico and northward to Wyoming. The SAGE II data during this period do not show any corroborating areas of clean air, nor are there any significant changes in the variance of the SAGE extinction measurements. Thus there are no simple explanations for this observation of surprisingly low concentrations at 0.25 μm between 20 and 25 km.
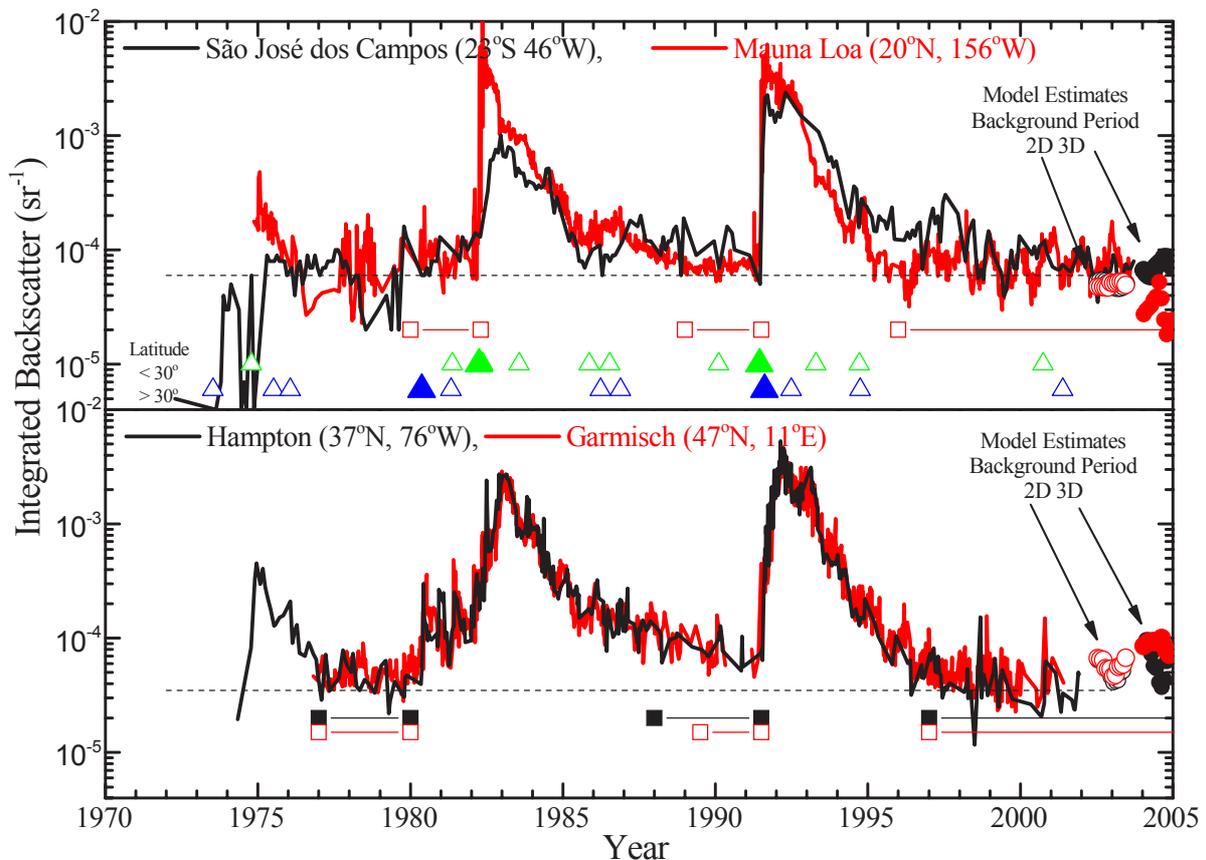
Histories for the integrated backscatter from the tropical and mid latitude lidars are shown in Figure 5.3. The tropical lidars use an integration beginning at 16-17 km whereas the mid latitude lidars use the tropopause or tropopause + 1 km as a beginning. Integrations extend to above 30 km. Both 2-D and 3-D model estimates of aerosol size distributions were used, along with Mie theory, to estimate integrated backscatter over one year in background conditions. These estimates for the lidar locations and wavelengths are shown between 2003 and 2005 in Figure 5.3.

The extremely low São José measurements prior to 1975 have been compared to northern hemisphere measurements in the same time period [Clemesha and Simonich, 1978]. The São José 20 km aerosol backscatter, β_a, was about half that measured in the northern hemisphere
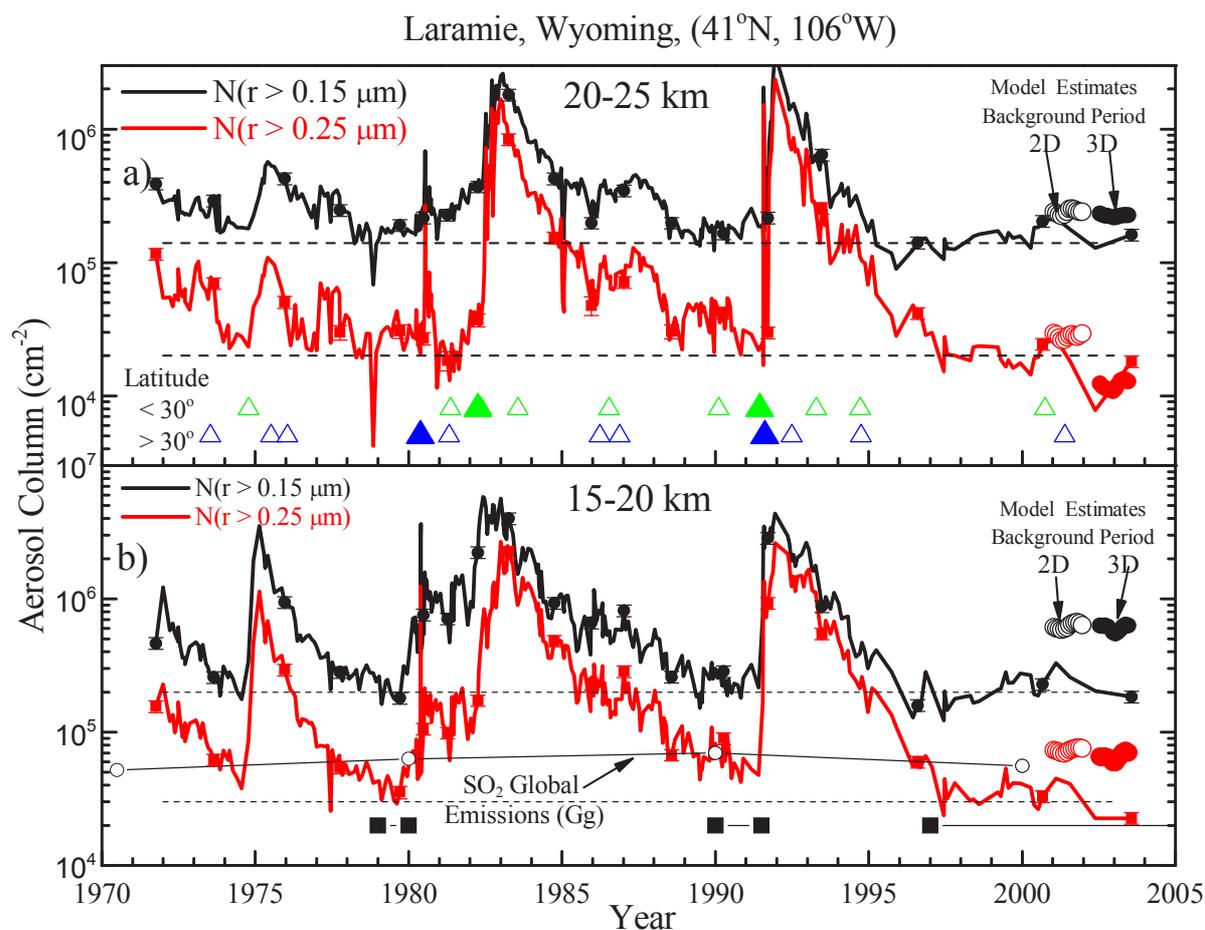
Figure 5.2. History of column integrals of aerosol number for particles with radii > 0.15 and > 0.25 μm from in situ measurements above Laramie, Wyoming, USA. The measurements represent about 340 individual aerosol profiles. The error bars on the occasional measurement represent the counting error of the measurement and rarely exceed the size of the data symbol. a) 20-25 km, b) 15-20 km. The dashed lines are horizontal and are meant only to aid the reader. The times of the most significant volcanic eruptions during the period are indicated with triangles in a), separated into those eruptions at latitudes less (upper symbol) and greater (lower symbol) than 30°. Eruptions with VEI of 5 (large closed symbol) and 4 (small open symbol) are shown. Names of the eruptions are listed in Table 1. Global emissions of SO_2 (Gg of S) are shown in b) for 1970-1990 [van Aardenne et al., 2001]. The scale for aerosol column also applies for Gg of sulfur. The 2000 estimate is based on a 20% decrease since 1990. The regions bounded by boxes in the bottom of a) and b) represent investigator determined background periods. Estimates from a 2-D (open symbols) and 3-D (closed symbols) model of background aerosol levels over one year are shown between 2000 and 2003 in both a) and b).

in 1973 using an airborne lidar operating at nearly the same wavelength [Fernald and Schuster, 1977]. Better agreement was found when β_a from São José was compared with β_a calculated from in situ aerosol measurements at 41°N in the same time period [Pinnick et al., 1976]. Only the Hampton, Virginia, lidar measurements extend into 1974, and these are in general quantitative agreement with the upper range of the early São José measurements. The suggestion from the São José measurements, of the lowest aerosol loading in the record prior to 1975, is not, however, corroborated by similarly low in situ measurements, Figure 5.2. This

Figure 5.3. History of integrated backscatter from two tropical sites (São José dos Campos and Mauna Loa) and two mid latitude sites (Hampton and Garmisch). The wavelengths for all measurements are 694 nm except for São José which is at 589 nm. Top panel: São José dos Campos, Brazil, integration from 17 - 35 km, and Mauna Loa, Hawaii, USA, integration from 15.8 - 33 km. Bottom panel: Hampton, Virginia, USA, integration from tropopause to 30 km, and Garmisch-Partenkirchen, Germany, integration from tropopause+1 km to layer top. The dashed lines are horizontal and are meant only to aid the reader. The times of the most significant volcanic eruptions during the period are indicated in the top panel with triangles, separated into those eruptions at latitudes less (upper symbol) and greater (lower symbol) than 30°. Eruptions with VEI of 5 (large closed symbol) and 4 (small open symbol) are shown. Names of the eruptions are listed in Table 1. Error estimates range from 5 to 50% and are somewhat dependent on the aerosol load. The regions bounded by squares in the bottom both panels represent investigator determined background periods for Mauna Loa, Hampton, and Garmisch. Results from two model (2-D, open symbols, and 3-D, closed symbols) estimates for integrated backscatter at 694 nm in one year of background conditions are shown between 2003 and 2005 for the lidar locations.

difference may be partly explained if the early São José measurements were biased low due to an undetected problem with the instrument in use at that time, or if there was a hemispheric difference in aerosol loading in 1974. Clemesha and Simonich [1978] suggest the Fuego aerosol did not appear in the southern hemisphere until April 1975 due to the inhibition of eddy transport in 1974 by the meridional circulation in northern winter. Even with this inhibition, there is, however, some suggestion of Fuego aerosol at São José in 1973. Although the early integrated backscattering is below the post-Fuego period, there is an aerosol increase

in late 1973, following the early 1973 Fuego eruption, and again in early 1975, following the late 1974 Fuego eruption, which appears to be the largest of the three eruptions.

The São José measurements in the early 1980s, prior to El Chichón, are in agreement with the Mauna Loa measurements. São José shows a smaller peak and faster decay after El Chichón, but similar peak backscatter and slower decay following Pinatubo. São José measurements are slightly elevated in the background period prior to Pinatubo compared to Mauna Loa measurements and to São José measurements in the period following Pinatubo. The similarity of the fluctuations between São José and Mauna Loa in the 1998 - 2002 period is striking. From the Mauna Loa lidar, the pre- and post-Pinatubo periods are similar, although the variation of the signal in the pre-Pinatubo period is much less than post Pinatubo variability. For the São José measurements the pre- and post-Pinatubo periods are both characterized by significant fluctuations.

The mid latitude lidars are in quite good agreement throughout the record. The peak integrated backscatter following Pinatubo and El Chichón are similar as are the decay rates. The relaxation of the stratosphere following El Chichón is delayed by several minor eruptions. This feature is also apparent in the in situ measurements particularly in the 15-20 km column. Considering the background periods, both lidars agree suggesting that the pre-El Chichón and post-Pinatubo periods are similar, whereas the pre-Pinatubo period is elevated. This again is similar to the in situ measurements particularly for the 0.25 μm measurements between 15 and 20 km. This correspondence between in situ 0.25 μm measurements and integrated lidar backscatter has been noted before [Jäger and Hofmann, 1991; Hofmann et al., 2003].

Comparisons between measurements and models, and between the 2- and 3-D models, are varied. Both model estimates for São José agree with each other and the measurements. For Mauna Loa the 2-D model agrees with measurements while the 3-D model is a factor of two lower. For the mid latitudes the model estimates are self consistent, but between a factor of 1.2 - 1.8 above measurements. This is consistent in direction, if not magnitude, with the model comparisons with in situ measurements. The model simulations in both Figures 5.2 and 5.3 are for a generic background year. The slightly different placements in the two figures are dictated by the space available in the figure.

Optical depths for zonally averaged SAGE and SAGE II aerosol extinctions at 1020 nm over the period 1984 - 2001 are shown in Figure 5.4. The data are zonal averages binned in 10° latitude intervals at the Equator, ±20° and ±40°. The base altitude, 18 km, was chosen to remove any influence of tropospheric aerosol or clouds. These figures show the decaying volcanic signal of El Chichón followed by the strong increase then decay in optical depth following the eruption of Mt. Pinatubo. The optical depth decreases with increasing latitude due to the fact that tropopause height decreases away from the equator, and background aerosol loading decreases with altitude above the tropopause. Thus optical depth for a constant altitude range will decrease with latitude. The difference between the Northern and Southern Hemispheres is within the random uncertainty which is typically ± 20%. The major exceptions to this are during the Pinatubo peak, for altitudes from 24 to 29 km, when aerosol was still forming, and in 1990 when Kelut is primarily only seen in the southern hemisphere. The difference following Pinatubo is most likely explained by stronger transport into the winter hemisphere from the tropics.
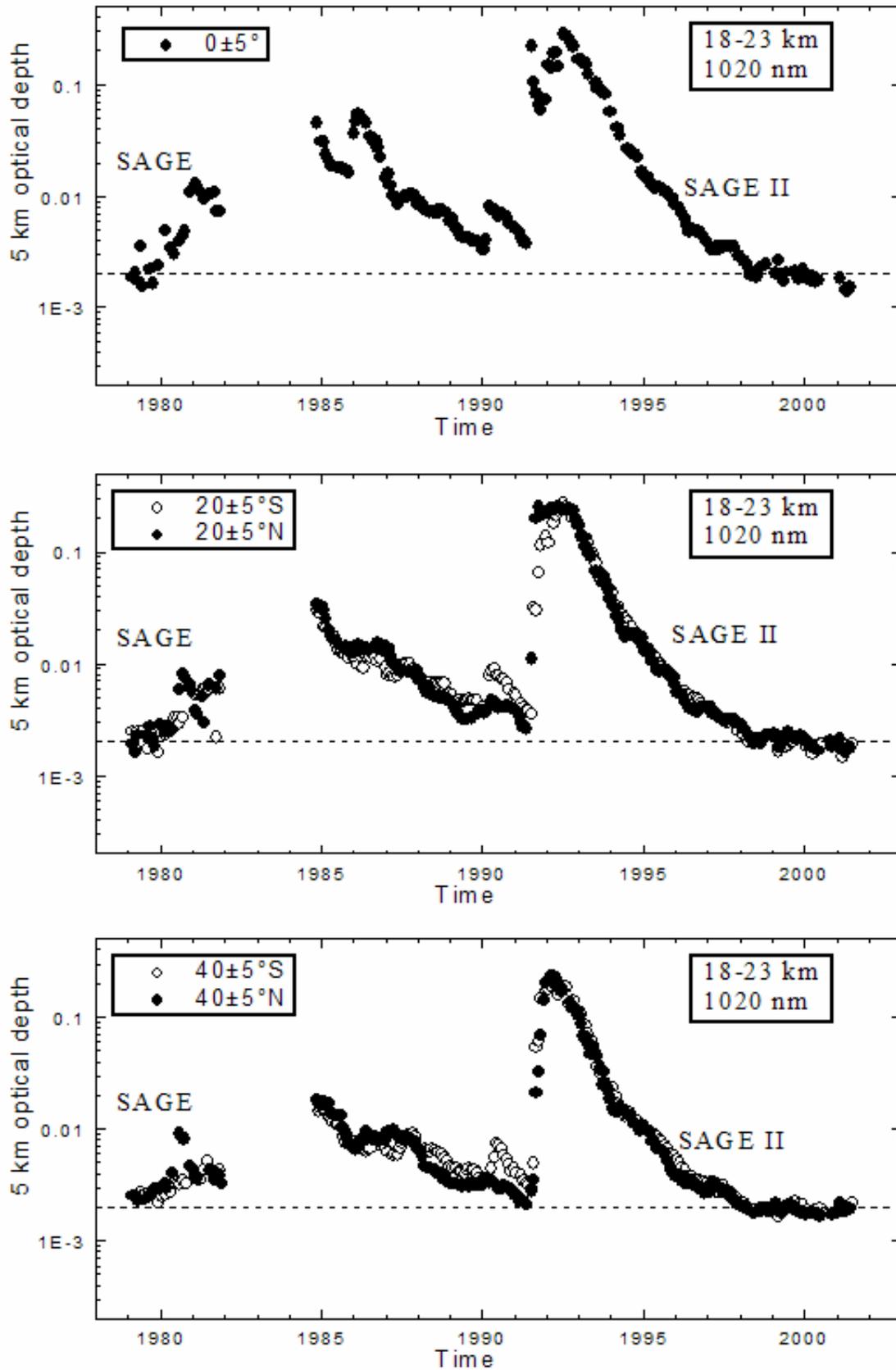
Figure 5.4. Zonal averages, ± 5°, of SAGE and SAGE II 1020 nm optical depths versus time centered at 0, ±20 and ±40°. Optical depth integrated from 18 to 23 km. Open (closed) symbols are for the Southern (Northern) hemisphere.
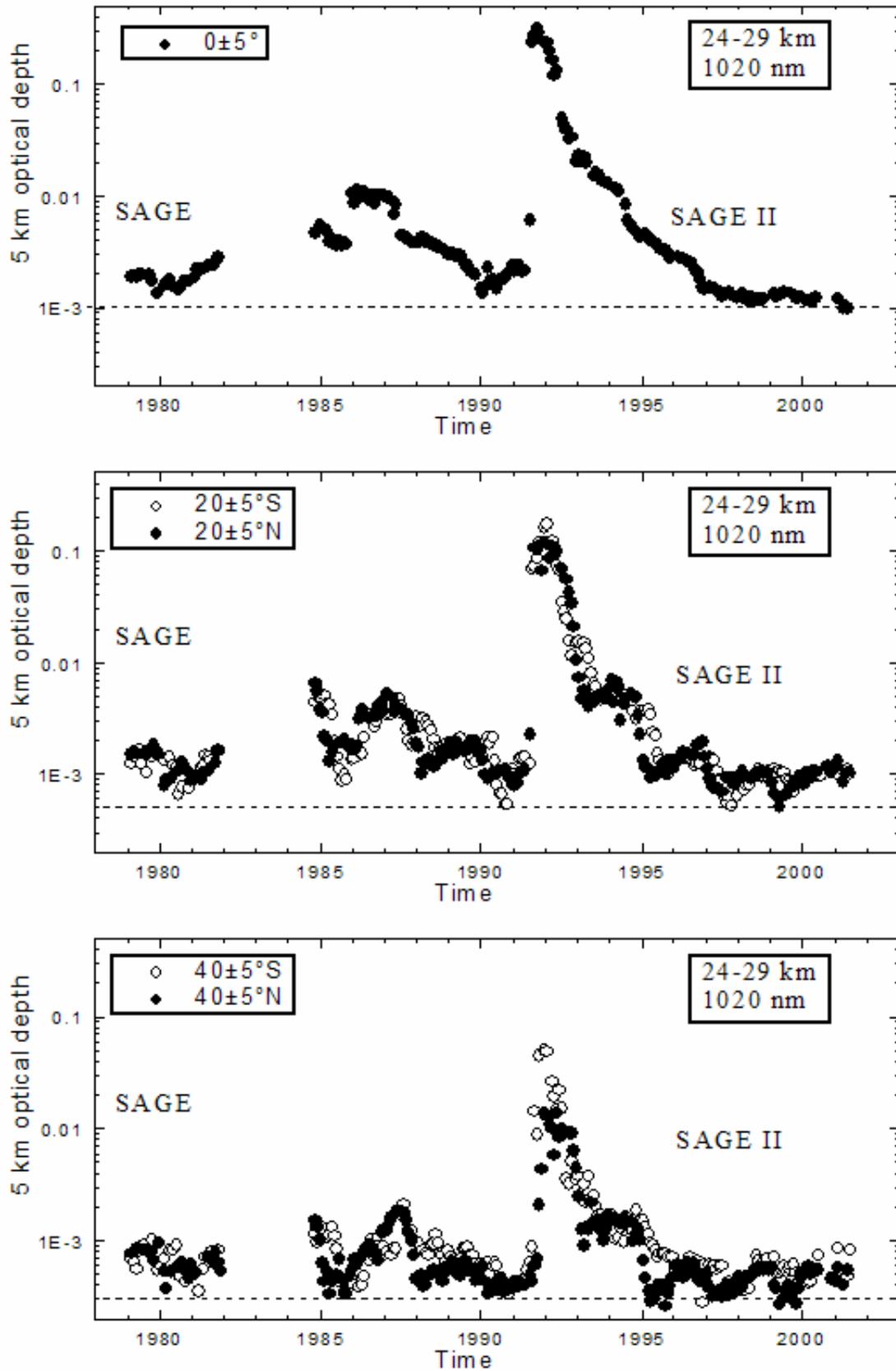
Figure 5.4 (cont.). Zonal averages, ± 5°, of SAGE and SAGE II 1020 nm optical depths versus time centered at 0, ±20 and ±40°. Optical depth from 24 to 29 km. Open (closed) symbols are for the Southern (Northern) hemisphere.

5.4   Investigation of trends in the long term aerosol measurement records

Previous analyses of long term trends in background stratospheric aerosol have been limited to comparisons of the aerosol record during volcanically quiescent periods. The first of these analyses [Hofmann and Rosen, 1980; Hofmann and Rosen, 1981; Sedlacek et al., 1983] compared measurements in the 1970s with Junge's [1960] initial measurements. The increase that these investigators reported can be seen in Figure 5.1 where Junge's initial 0.15 μm concentration measurements [Chagnon and Junge, 1961] are compared with the long term Laramie record. Figure 5.1 also indicates that in the mid latitudes in the 1970s the periods when stratospheric aerosol may have reached background were short, ~1-2 years.

Table 5.1 lists the time, location, VEI, and aerosol load if available, for all volcanoes with a stratospheric impact, generally VEI ≥ 4, since 1960. The 1970s were dominated by one large tropical eruption, Fuego, and no small tropical eruptions. All other eruptions were at high latitudes. In contrast the 1980s were dominated by one large tropical, El Chichón, and several smaller tropical eruptions. The smaller tropical eruptions, particularly Nevado del Ruiz and Nyamuragira, interrupted the decay from El Chichón and led to some controversy about whether stratospheric aerosol had reached background prior to Pinatubo [Hofmann, 1990; Thomason et al., 1997]. This discussion highlights an uncertainty in knowing if and when the lowest background loading is present. In hindsight it now seems clear, based on the volcanically quiescent period following Pinatubo, that background was not reached prior to Pinatubo [Barnes and Hofmann, 2001; Hayashida and Horikawa, 2001], Figures 5.2, 5.3, 5.4.

The statistical analysis here will follow two approaches. The first will follow the lead of previous investigators and compare the 3 volcanically quiescent periods in the 5 long term data sets which capture these. The second will use an empirical model to remove the volcanic signal from the long term records and investigate the residuals for trends. This approach permits the SAGE data to be included. These analyses do not account for the impact of trends in stratospheric water vapor and temperature on aerosol size, but this appears to be minor. The main problems with these approaches are technical. Temporal autocorrelations, present in all data, violate standard statistical independence assumptions. Proper analyses that account for autocorrelation indicate much smaller effective sample sizes, and confidence bounds on estimates are consequently inflated. Also, maximum likelihood estimation with mixed models including autocorrelation parameters is occasionally unstable, and estimation algorithms may fail.

Given sulfuric acid mass, water vapor pressure, and temperature, the composition of stratospheric aerosol can be predicted from thermodynamics [Steele and Hamill, 1981]. Using aerosol composition and assuming a lognormal size distribution with constant width, the mode radius of the aerosol can also be predicted. Since over the record of long term stratospheric aerosol measurements there have been increases in stratospheric water vapor and decreases in stratospheric temperature, both of which would lead to larger particles, the effects of these changes were estimated to see if they were significant. Since the 1950s there has been approximately a 1% yr^{-1} increase in stratospheric water vapor [Oltmans and Hofmann, 1995; Kley et al., 2000] and approximately a 0.5 K per decade cooling of the lower to middle stratosphere [Ramaswamy et al., 2001]. These changes in water vapor and temperature were used to estimate the fractional change in particle size and composition. The changes were found to be negligible, less than 10^{-4} μm $decade^{-1}$ in size and -0.5% $decade^{-1}$ in composition in the lower to middle stratosphere between 70°S and 70°N. These changes of aerosol in volcanically quiescent periods are not observable in the measurements available for

comparison. In addition Nedoluha et al. [2004] suggest the trend in water vapor may not be as high as 1% yr^{-1} leading to even less of a change in aerosol size.


5.4.1   Comparison of stratospheric aerosol during non volcanic periods

The results of a comparison of measurements in background periods will depend in large measure on how the periods are specified. While defining background periods is relatively straight forward, specifying background periods can be fraught with difficulty since: a) most stratospheric volcanic aerosol decay processes display an exponential rather than linear character, b) there can be input from minor eruptions between major eruptions, such as after El Chichón, c) recent history has been relatively volcanically active, and d) the time periods for some background periods can be exceedingly short. Between 1971 and 1997 at least 70% of the sampling period was perturbed by volcanic activity.

In spite of these difficulties the in situ, 15-30 km column, and lidar, integrated backscatter, measurements are used to compare the measurements during the three background periods identified for each data set. This analysis is completed because it is straight forward and has been the approach of all preceding analyses of background stratospheric aerosol. The background periods were identified by each investigator based on their individual criteria, Figures 5.2 and 5.3. While a more objective approach would be preferable, the variation in the measurements and the sometimes brief background periods are not amenable to a more objective analysis. The approach followed allows experimentalists, using their understanding of the measurement technique, and characteristics of stratospheric aerosol, to manually inspect the record and select time periods free of volcanic aerosols. Although this method is the most subjective, it benefits from the investigator's experience in recognizing the effects of volcanic activity. The method relies on a subjective assessment of when the characteristic decay of aerosol mixing ratio or integrated backscatter, following a volcanic eruption, no longer influences the record. The background periods identified by the experimentalists at Hampton and Garmisch are equivalent except prior to Pinatubo (Figure 5.3b), adding some credibility to investigator determined background periods. The background periods for Mauna Loa were used also for the São José dos Campos data, except after Pinatubo, then the São José dos Campos background period was begun in 1998.5. Prior to 1997 the background periods identified for the in situ data are quite short. The sensitivity of this analysis to the choice of background periods was tested by changing the background periods selected by ± 0.5 yr. These changes did not significantly affect the results.

The comparisons of background periods were completed using analysis of variance with adjustment for autocorrelation to compare the data within each of the three background periods for each data set, and by applying a linear regression model to the log of the aerosol measure versus time to investigate temporal changes in the background periods. Figure 5.5 presents for each data set, the background data, means and 95% confidence intervals for measurements during each background period, and the results from a linear regression model applied to the data.

The analysis of variance tests indicate little difference between the means of the first and third background periods. A statistically significant increase was observed for the middle period, pre-Pinatubo, for the Laramie-0.25 μm, Garmisch, and Hampton data. This increase in the background prior to Pinatubo has been discussed by Hofmann [1990] and Thomason et al. [1997] and is clearly evident in the high northern latitude sites in Figure 5.5, except for the
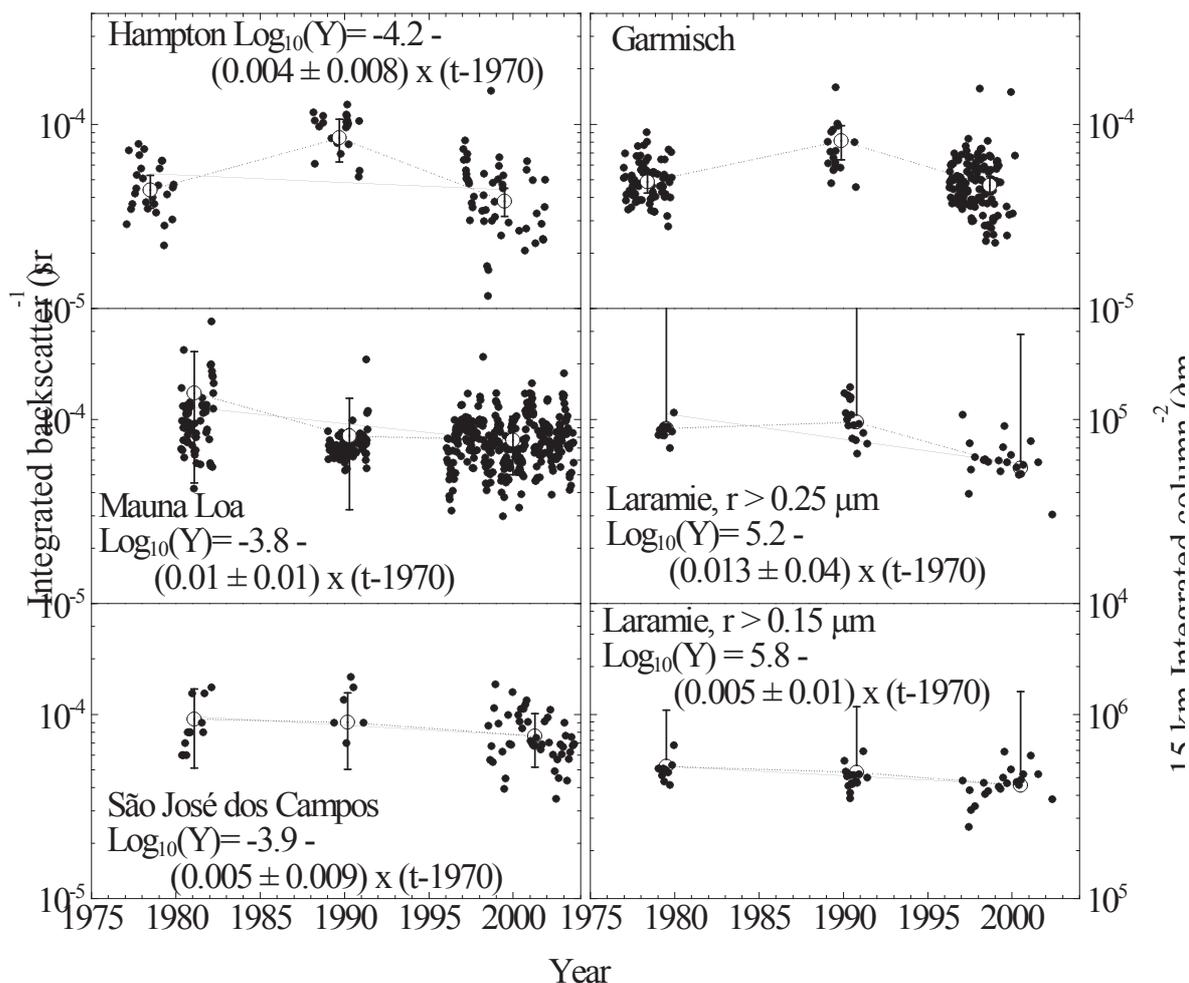
Figure 5.5. Comparison of measurements during three investigator determined background periods for integrated backscatter measured above Garmisch, Hampton, Mauna Loa, and São José dos Campos, and for column integrals, 15-30 km, of aerosol concentration for particles ≥ 0.15, 0.25 μm above Laramie. Means and 95% confidence intervals, with adjustments for autocorrelation, for each background period are shown (symbols with error bars connected with a dashed line) along with a linear regression (solid line) when convergence, including autocorrelation, was achieved. This the case for all but Garmisch. The log of the regression equation is shown with 95% confidence intervals for the slope of the equation The interval on the ordinate for each graph is the same so that even though magnitudes of the aerosol measure differ between the lidar and in situ measurements, the slopes are comparable.

Laramie-0.15 μm data. It now seems clear that this period was still perturbed by residual volcanic activity, either from Kelut in 1990 or remnants from Nyamuragira or Nevado del Ruiz in 1986. The other site to show a non-zero difference with this analysis is Mauna Loa where the data suggest that the first background period is elevated compared to the pre- and post-Pinatubo periods, which show no significant difference. No difference is apparent for any period for the Laramie-0.15 μm and São José dos Campos measurements.

The linear regression for the three background periods analyzed suggests trends and 95% confidence intervals of -0.5 ± 1.0 % yr^{-1} for the Laramie 0.15 μm, Hampton, and São José dos Campos measurements, -1 ± 1.0 % yr^{-1} for Mauna Loa measurements, and -1 ± 4.0 % yr^{-1} for Laramie 0.25 μm measurements. Mixed model linear regression estimation for Garmisch

failed to converge. If autocorrelation is ignored confidence intervals are smaller and these results suggest a negative trend in stratospheric aerosol for the Laramie 0.25 μm and Mauna Loa measurements, which is significant. The data, however, are not independent. Autocorrelations at the scale of one month were estimated between 0.70 and 0.98, values which strongly affect inference. The autocorrelation is high because, on the time frame of one month, and away from large volcanic eruptions, the stratospheric aerosol content changes slowly, and thus a measurement in one month is a good predictor for the following month. Unequal time spacing and the autocorrelations were accommodated by appealing to a one-dimensional spatial model, equivalent to a first-order autoregressive error regression model. The results are compelling in that data which suggest changes in background without accounting for autocorrelations (Laramie-0.25 μm, Mauna Loa, Figure 5.5) do not suggest any trend when autocorrelation is accounted for. Although estimates of growth/decay rates change little, standard errors typically about triple when autocorrelations are included which is the more appropriate model for these data sets.

This analysis follows the lead of the early comparisons of background periods, but concludes that there is no long term trend in background aerosol. This is in agreement with other recent comparisons of background periods using single data sets [Barnes and Hoffman, 1997, 2000, Deshler et al., 2003; Jäger, 2005]. Care, however, must be exercised to limit the confidence in conclusions drawn from comparisons which include just a few epochs containing background data. In particular the conclusion from this analysis is dependent on confidence that stratospheric aerosol had reached background in 1979-1980, prior to Mt. St. Helens. This period is quite short.

5.4.2   Removing the volcanic signal from the long term measurement records

The second approach to analyze for trends in background aerosol seeks to remove the major perturbing signal, the volcanic effects, from the data. The resulting baseline is then analyzed for trend. This approach uses techniques applicable to a wide range of observations and does not require a priori knowledge of the unique behavior of a particular data record. The advantage of this approach is to transform the long term, ~30 year, measurement records from ones limited to comparisons of 2-3 time periods, which range from 1 to 5 years, to a record which includes the entire time period of measurements. Considering that the longest satellite record, SAGE II, captures just two non-volcanic periods this is practically the only approach that can take advantage of this global 20 year record. The four lidar records and one in situ record capture three background periods, which comprise ~40% of the measurements at these sites, with the post Pinatubo background period encompassing 20%. Thus, prior to Pinatubo, ~80% of the measurements were completed during volcanically perturbed periods.

 The disadvantages of such an effort is that no simple model of volcanic aerosol growth and decay can accurately capture all of the processes involved in the dispersal and removal of volcanic stratospheric aerosol as reflected in each of the various long term measurements. This, however, does not preclude the application of an empirical model to remove the majority of the variance of the aerosol signal produced by volcanic eruptions. Such a model will be inherently tied to each measurement set and can only be applied to that measurement set. Application to a different set of measurements will use the same conceptual model but require a new set of empirical parameters.

The following considerations guided the choice of an empirical model to remove the volcanic influences: (1) The 1-2 order of magnitude changes in aerosol signal from background to volcanic period suggest a log transform of the measurements to avoid excessive weighting of

the volcanic period. (2) The roughly linear decay of any of the aerosol measures plotted in Figures 5.2 and 5.3, on a log scale, suggests a roughly exponential decay of volcanic aerosol. This assumption has some problems as background aerosol levels are approached, but is generally valid and has been used often [Yue et al., 1991; Rosen et al., 1994; Osborn et al., 1995; Deshler et al., 1997]. (3) When modeling the process some attention must be given, at each site, to the time lag between an eruption, the time the initial aerosol pulse arrives and the period of time leading to the peak aerosol signal. The latitude of the observation site with respect to the volcano and the season will influence this, e.g., compare the arrival of El Chichón and Pinatubo aerosol at the four lidar sites shown in Figure 5.3. The transitions are characterized by both a time lag until the aerosols arrive and a buildup period from initial impulse to peak signal. Both the lag and the buildup are extended for more distant sites. 4) Cumulative effects of volcanic inputs and background sources are assumed to be additive. 5) The nature of the data is such that some variation in the measurements is fairly constant (measurement uncertainties), and some increases with scale (local natural variations following large volcanic eruptions). Variation that increases with aerosol signal appears during and following volcanic inputs. Figure 5.6a, displaying the Garmisch lidar measurements on a linear scale, illustrates this point. The variations which increase with integrated backscatter dominate the variance of the signal. Because these effects dominate, it is natural to use a log scale to display data as in Figures 5.1-5.4. 6) It is assumed that there is a non-volcanic, background, component to stratospheric aerosol which would exist in the absence of volcanic eruptions. Based on the data this assumption is reasonable, certainly more reasonable than assuming there is no background aerosol. Explicit inclusion of a term for a baseline in the model is also more consistent with the data than is exclusion of the term. The goal of the modeling exercise is to determine if the background aerosol level has changed, or remained constant, over the course of the measurements. Displays on log scales indicate the data are approximately lognormally distributed. Measurement error and perhaps some of the natural variation, however, exists at a fairly constant level and is approximately normally distributed. The true total "error" in the data is thus probably a convolution of normal and lognormal components, but, overall, the lognormal effects dominate and a simple lognormal model to remove volcanic signals is used.

Based on these considerations the following empirical model is developed for log(Y(t)), where Y(t) is a time dependent aerosol measurement from any of the long term records. Plots of log(Y) versus time for the aerosol measurements under consideration are shown in Figures 5.2-5.4. The empirical model has the form:

$$\log\{Y(t)\} = \log\{ B \exp(\beta t) + \sum_{1}^{N} V_j(t) \} + error. \qquad (5.1)$$

The initial term $B \exp(\beta t)$ allows for an overall trend of the baseline, a value of $\beta = 0$ implies a constant baseline at B, whereas positive and negative values of β represent respectively growth and decline in background levels. The proposed model is thus based on a possibly changing baseline plus a chain of events added together over time. The number of measurable volcanic inputs over the observation period is determined by inspection from the data. Each volcanic input $V_j(t)$ consists of two parts, one for an initial, finite transition period during which aerosols are arriving, and the other for an open-ended period of decay. Exponential decay is assumed to be operative during both periods, although arrival dominates decay during the (usually brief) transition period, and only decay is present for the second period. In the second, more important period, starting at time τ_{jz}, the function is of simple form $P_j \exp(-v_j (t-\tau_{jz}))$ where P_j is the aerosol load at time τ_{jz} and v_j is the volcano dependent

exponential decay rate. The decay parameters ν_j are assumed positive, whereas β (the background growth or decay) can be positive or negative.

The first period (transition) is less consequential but more complex. It is assumed that arrival of aerosols follows a positive continuous function $Q_j(t)$. These functions are modeled with three parameters: the time of appearance of volcanic aerosol at a site, τ_{ja}, the time when aerosols cease arriving, τ_{jz}, and the peak level of the wave over this interval, P_j, which may be shown to occur at τ_{jz}. Knowledge of event times puts a lower bound on each τ_{ja}. Assuming that the exact form of the wave is not critical, a truncated quadratic fixed at zero before τ_{ja} and after τ_{jz}, inclusive, is used. For time t between τ_{ja} and τ_{jz} the mean aerosol level is then $\int_{\tau_{ja}}^{\tau_{jz}} Q_j(t) \exp(-\nu_j(t-\tau_{ja}))\, dt$. The integral has a closed form that is perhaps unnecessarily
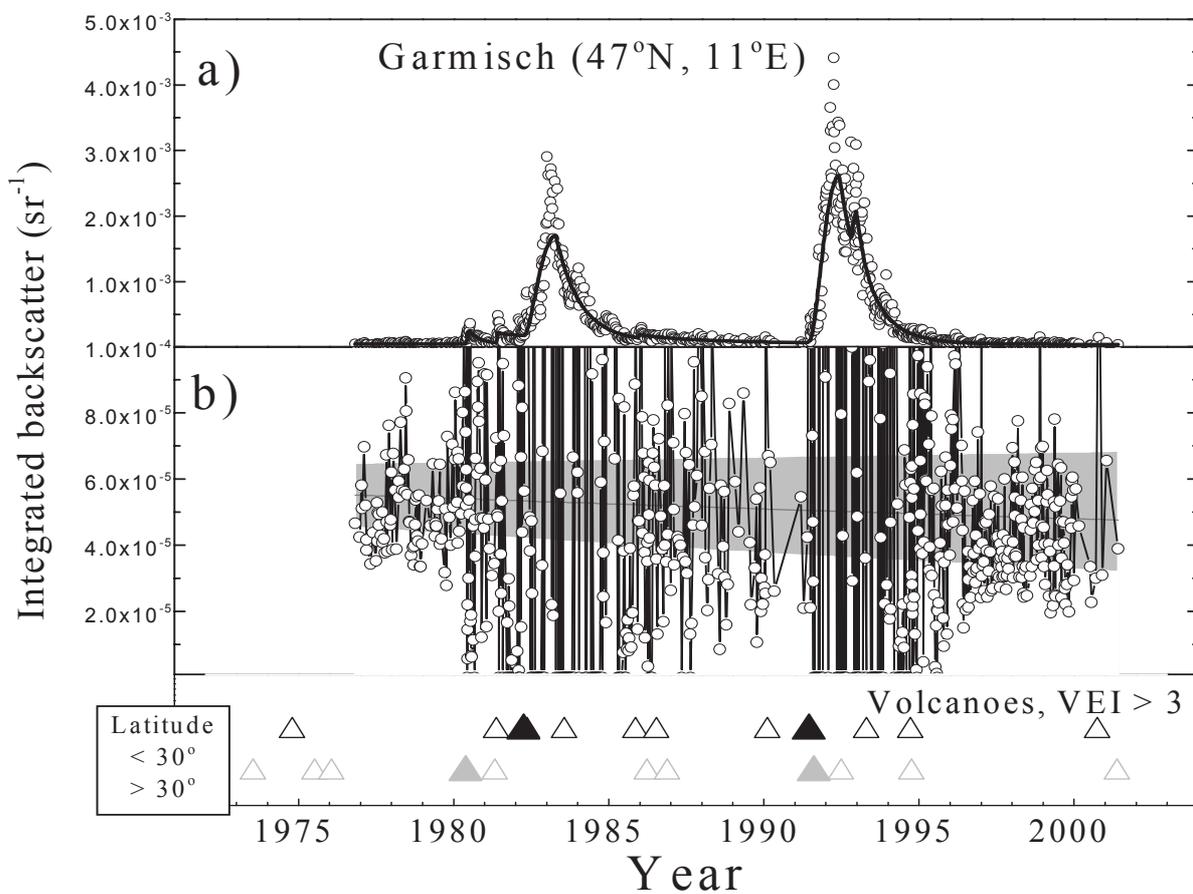
Figure 5.6. (a) Integrated backscatter (data points) from Garmisch, compared with the parametric model (solid line) for Garmisch, plotted on a linear scale. Compare the large variations near the peak of aerosol load for either El Chichón or Pinatubo with the variations of measurements near background. (b) Integrated backscatter for Garmisch with the modeled volcanic effects removed. Values become large and sometimes negative near the eruptions of El Chichón and Pinatubo due to the large natural variations around the volcanic model. Also shown are the mean and ±95% confidence limits for the modeled baseline and its trend.

complex, but it has the virtue of being parsimonious with respect to the parameters required for any one volcano and all parameters have physical interpretations.

For N volcanoes the model has 4N+2 parameters, four for each volcano and two for the baseline. The chief drawback of this model is not, however, its dimension but rather the fact that conventional fitting is almost impossible to do exactly. The time limits τ_{ja} and τ_{jz} interject breaks in the smoothness of the function, and convergence is not feasible without unconventional optimization methods or else careful monitoring and coaching of the process. For current purposes, a near optimal fit is satisfactory, because the primary purpose of the modeling is to allow volcanic inputs to be removed, leaving a baseline which can be assessed for trend, Figure 5.6b. The residuals are highly autocorrelated over time, and consequently simple linear regression trend analysis is not reliable in terms of inference. The degree of statistical significance is expected to be strongly inflated in these circumstances, so assessment of trend is done using a model that allows for first order autocorrelation. Data are unequally spaced in time, so analysis is performed using a one-dimensional spatial representation instead of a standard time series analysis [Cressie, 1993]. The clustering of points below the baseline and gray area between 1996 and 2000 in Figure 5.6b is somewhat misleading. It is partly an artifact of the linear fit, partly due to the vertical truncation in 5.6b to emphasize the character of the gray area, and partly due to autocorrelation of the data. The vertical truncation masks some influential outliers above the gray area which are carrying a substantial part of the balance. Because of autocorrelation the thick clustering of points recorded between 1996 and 2000 are not as influential as they appear. With unequal time spacing, in particular, counting numbers of points can be deceptive.

The optimization procedure uses a priori estimates for each parameter and then standard squared-error residual minimization to obtain the set of parameters providing the minimum in the residuals. Figure 5.6a presents the results obtained from a fit of the parametric model, Eq. (5.1), to the log of integrated backscatter from Garmisch. In this case 6 volcanic events were included so a 26 parameter model was used. The measurements compared to model estimates on a linear scale are shown in Figure 5.6a, while the aerosol signal with volcanic influences removed is shown in Figure 5.6b along with model estimates of the baseline trend with 95% confidence limits. The results of similar optimized fits to all of the lidar and the in situ measurements are shown in Figure 5.7, on a log scale to display variations during background periods. Also shown are model estimates of the baseline trend with 95% confidence limits (gray shaded area) and the times of volcanic eruptions with VEI ≥ 4. The boundaries of the shaded area are calculated from $Y(t) = (B \pm \Delta B)*\exp[(\beta \pm \Delta\beta)*(t - t_o)]$. The initial shaded area's finite width is set by ΔB, the uncertainties in B. This area grows because of the uncertainty in the time rate of change of the background, $\Delta\beta$, leading to an increase in uncertainty with time.

The model does a reasonable job of capturing the measurement variations through the volcanic perturbations. However, as apparent from Figure 5.7, not all volcanoes were included in the model for each site. Initially all volcanoes which appeared in the record were included. If convergence of the model was not achieved, then some of the smaller volcanoes were removed for that site and the model rerun. This process was repeated until convergence was achieved. Thus, for example, Nevado del Ruiz and Nyamuragira were not included in the São José dos Campos model, whereas Mt. St. Helens was not included in the Laramie records. Both the Laramie in situ data and Hampton lidar data were highly perturbed by Mt. St. Helens in comparison to other sites. This perturbation created difficulties in establishing a baseline prior to the eruption of El Chichón for the Hampton and Laramie data. Perhaps the proximity

of this volcano and the increased sampling frequency at Laramie and Hampton contributed to these difficulties. For this analysis only elimination of these data from the Laramie record permitted the model to converge at reasonable levels. This extreme step was not taken for the Hampton data, but it is clear from Figure 5.7 that the minimum in the measurements prior to El Chichón, is not modeled correctly for Hampton.
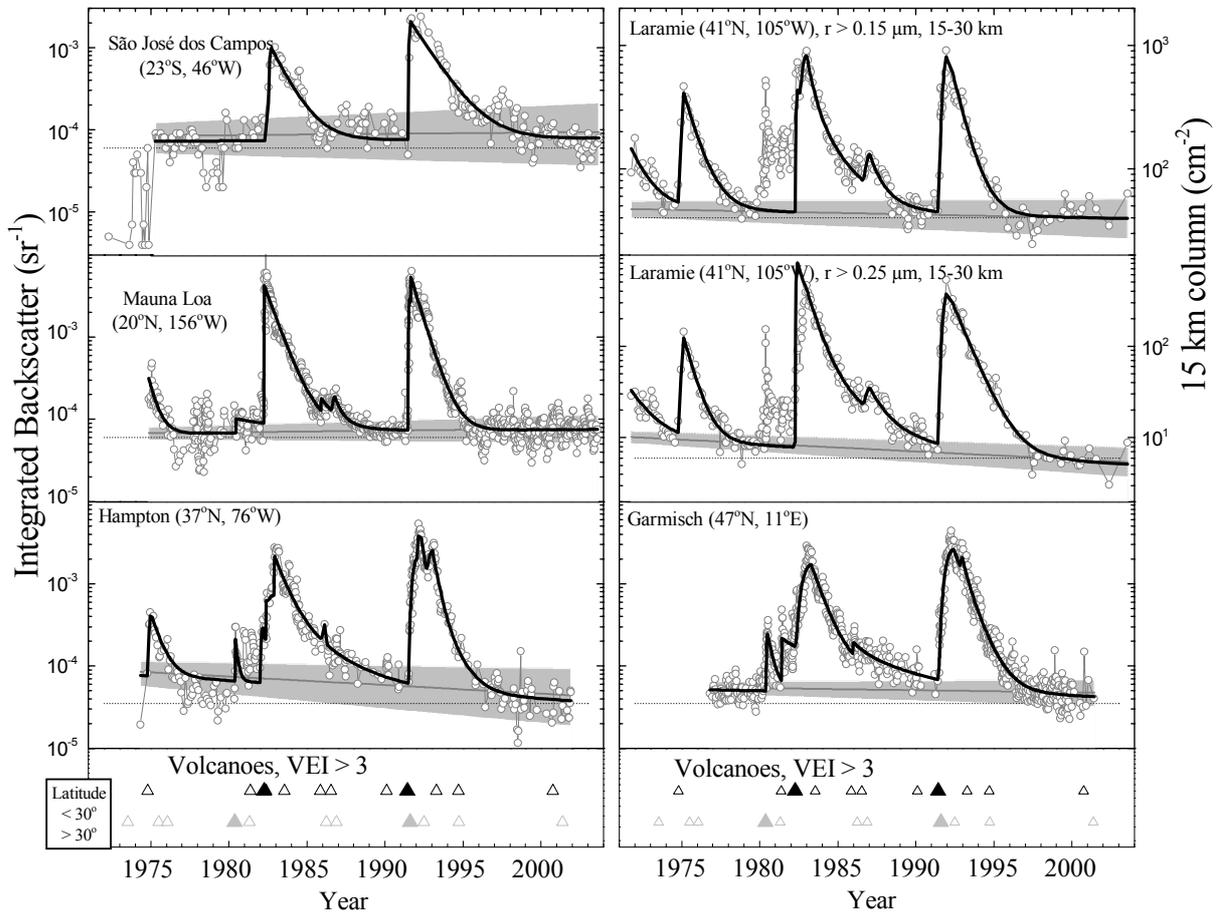
Figure 5.7. Integrated backscatter (data points) from São José dos Campos, Mauna Loa, Hampton and Garmisch lidar measurements, and integrated aerosol column (15-30 km) for particles with radius ≥ 0.15, 0.25 μm from Laramie compared with parametric model fits (solid lines) to the log of the measurements. The gray shaded areas provide the estimated background aerosol, with 95% confidence intervals, from the model. The time of volcanic eruptions with VEI ≥ 4 (open triangle) and 5 (closed triangle) are shown at the bottom divided into those eruptions at latitudes less than and greater than 30° of latitude, upper and lower symbols. The model was applied to the São José measurements beginning in 1975, and Mt. St. Helens was not included in the model for Laramie.

Table 5.2 provides the estimates of B, β, P_j and ν_j, along with their standard errors for each of the sites. The 95 % confidence limits on any parameter are given approximately by plus and minus two standard errors of the mean. Time parameters τ_{ja} and τ_{jz} are omitted from the table. The measurements with modeled volcanic signal removed for the lidar and two in situ records along with the baseline ± 95% confidence interval are shown in Figure 5.8.

Table 5.2. Parameters used in the parametric model used to estimate the measurements from each long term measurement site. The rate parameters have units of yr^{-1}. The standard errors of each parameter are indicated by σ. The 95% confidence intervals are given approximately by parameter ± 2σ. Note only the background fit parameters incorporate autocorrelation in the estimates of standard errors. This is not the case for the volcanic fit parameters. When multiple bursts are modeled for a single volcano, parameters for the slowest decay rate are recorded, and the value is marked with an asterisk.

Parameter		Laramie15	Laramie25	São José	MaunaLoa	Hampton	Garmisch
		15-30 km column (cm^{-2})		← Integrated backscatter × 10^4 (sr^{-1}) →			
Back-	B	47	10.0	0.83	0.68	0.85	0.55
Ground	σ(B)	3.7	0.76	0.15	0.061	0.15	0.049
	β	-0.0056	-0.020	0.0039	0.0045	-0.024	-0.0060
	σ(β)	0.0035	0.0035	0.0080	0.0039	0.0083	0.0042
Fuego	P	360	110	NA	2.9	3.7	NA
	σ(P)	34	12	NA	0.53	0.78	NA
	ν	1.1	1.5	NA	2.0	2.4	NA
	σ(ν)	0.093	0.13	NA	0.34	0.47	NA
El	P	500	840	8.20	41	18	15
Chichón	σ(P)	110	170	1.50	2.0	4.4	0.70
	ν	2.2	1.4	0.74	1.2	1.9	1.3
	σ(ν)	0.76	0.22	0.096	0.037	0.84	0.13
Pinatubo	P	810	390	21	28	17*	26*
	σ(P)	45	22	4.0	5.4	4.8	1.0
	ν	1.3	0.98	0.70	1.5	1.1*	1.2*
	σ(ν)	0.05	0.035	0.072	2.4	0.11	0.035

Based on Figures 5.7, 5.8 and Table 5.2 the change in the baseline, indicated by β, does not differ significantly from zero for the Garmisch, Mauna Loa, São José, and Laramie 0.15 μm records. Slight negative trends, ~2% yr^{-1}, are determined for the Hampton and Laramie 0.25 μm measurements. These results, suggesting a stable or at most a slightly decreasing, stratospheric background aerosol, are consistent with the simpler analysis of background periods discussed in section 5.4.1. Only the Laramie 0.25 μm measurements result in a slight negative trend for both types of analyses. The simpler analysis of background periods for Hampton data suggests no trend, with perhaps a slight negative trend for Mauna Loa. For the Laramie 0.25 μm measurements the parametric model estimate of background aerosol decreasing at ~2% yr^{-1} exceeds the ~1% yr^{-1} estimated in section 5.4.1. Errors in the measurements do not allow finer limits to be placed on possible changes.

A similar model was applied to SAGE II satellite data, the only satellite measurements with a history long enough to consider trends in background stratospheric aerosol. For this analysis the SAGE II extinctions were zonally averaged into ± 5° latitude bins and optical depths calculated in three 5 km altitude intervals, 18-23, 24-29, and 30-35 km. The latitude bins were centered at 0, ±10, ±20, ±30, ±40, and ±50°. This subdivision of the SAGE II measurements provided 33 data sets for each of the four SAGE II extinction measurements. These data are less complex than the lidar and in situ data since the time period covered is only two thirds of the lidar and in situ data and volcanic eruptions were less frequent during this period. The
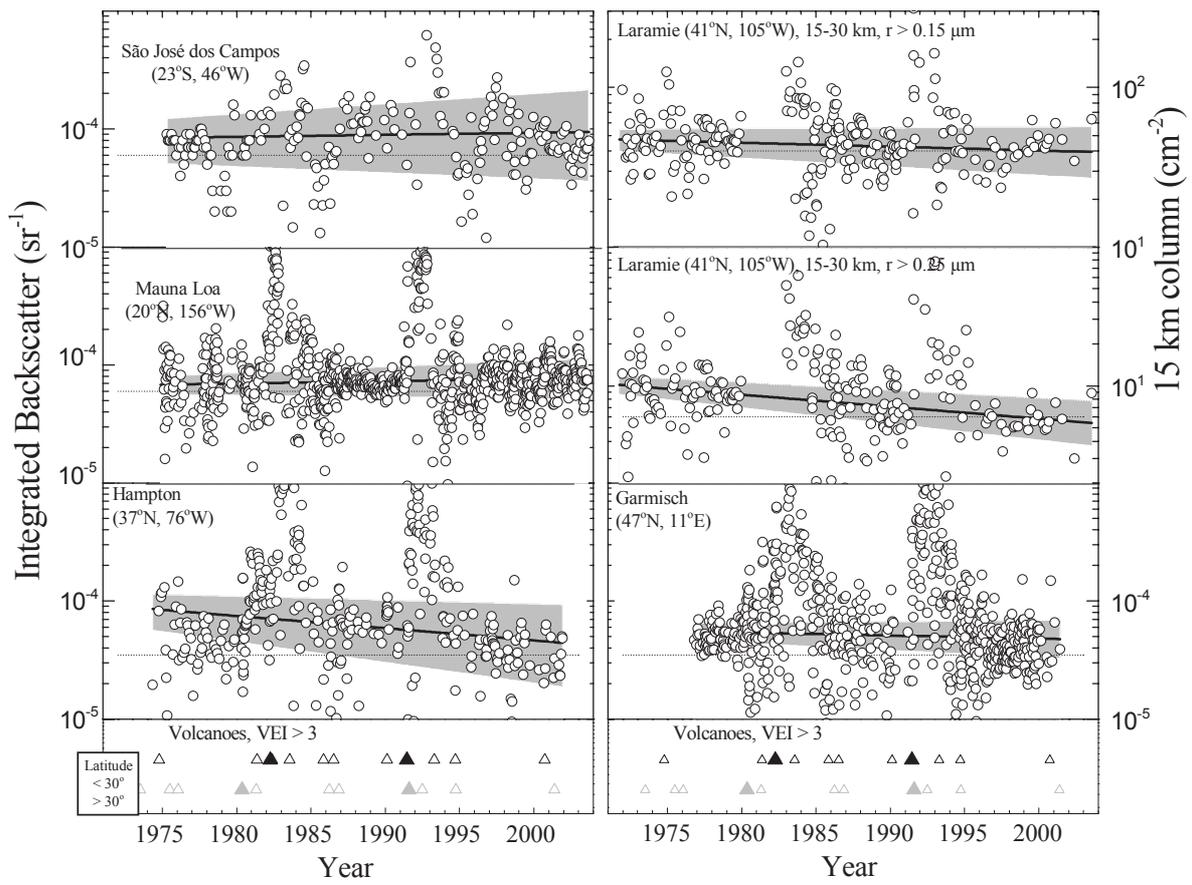
Figure 5.8. Same as Figure 5.7 except the data represent the differences between the measurements and the volcanic portion of the model. The residuals for Laramie in 1980, following Mt. St. Helens, are off scale since Mt. St. Helens was not included in the model for Laramie.

number of volcanic events included in models of the SAGE II measurements varied from 3 to 4 depending on latitude. The tropical eruption of Kelut, a year prior to Pinatubo, did not affect the high latitude measurements. The analysis was completed for all 33 data sets for the 1020 nm extinction measurements since this is the most stable SAGE II aerosol measurement. These results are expected to apply equally as well to some of the other wavelengths; however, care would be required if the shortest wavelength, 385 nm, was used. Time restraints prevented extending the investigation to the other three wavelengths.

Figures 5.9-5.11 present the results of parametric model fits to SAGE II 5 km optical depths for 5 latitude intervals and 3 altitude intervals. Figures 5.12-5.14 provide the SAGE II measurements with the volcanic signal removed compared with the baseline estimates. Figures 5.12-5.14, as Figure 5.8, include the removal of only the volcanic signal. Thus any changes in the background aerosol will appear in Figures 5.8, 5.12-5.14. The results are consistent with the ground-based lidar and balloonborne in situ measurements. The value of the change rate for background aerosol, β, is not, statistically, significantly different from zero for the 20 year SAGE II measurement record. The results shown for SAGE II are indicative of similar analyses at $\pm$ 10, 30, and 50°. These results highlight the usefulness of
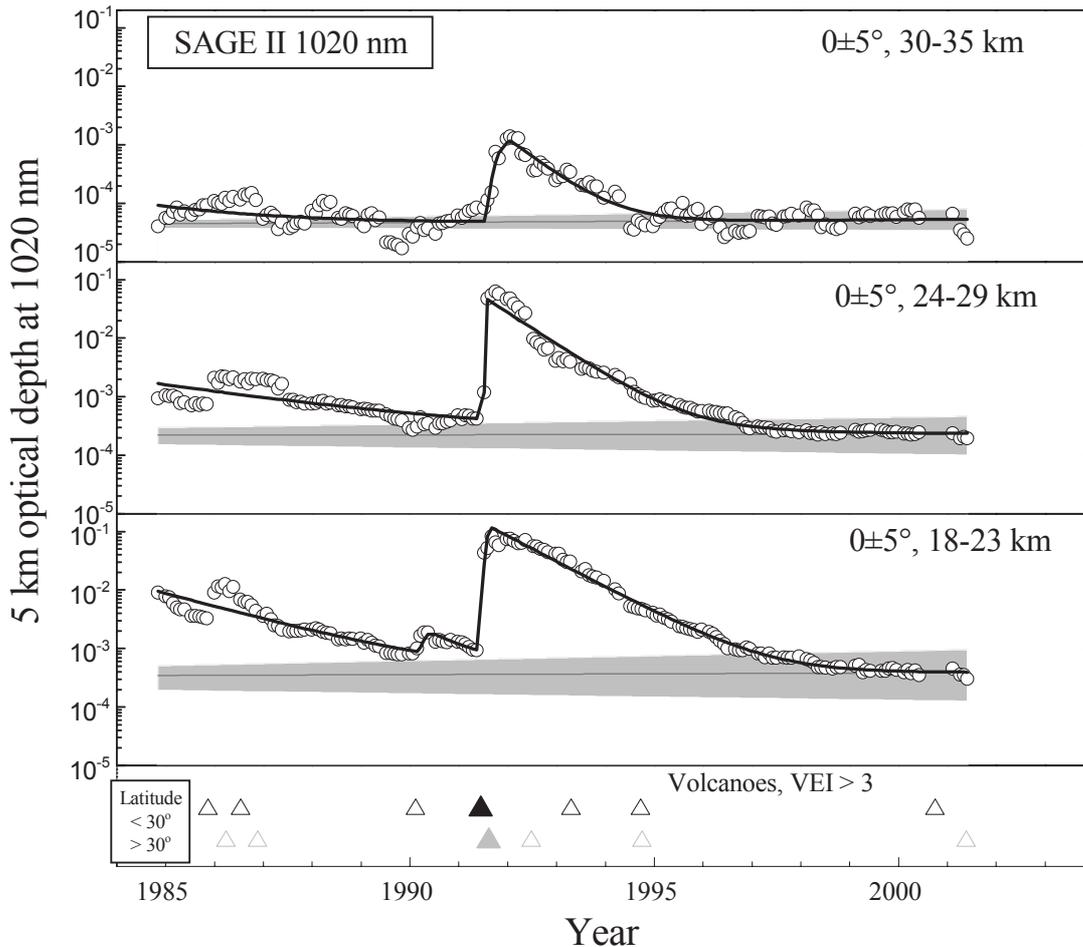
Figure 5.9. Optical depths integrated over three 5-kilometer altitude intervals for zonally averaged (±5°) SAGE II 1020 nm extinctions at a latitude of 0°, compared with parametric models fit to the data and with estimates of the baseline and trend for optical depth during background aerosol conditions. The estimated background is shown with ±95% confidence intervals as the gray shaded area. The time of volcanic eruptions with VEI ≥ 4 (open triangle) and 5 (closed triangle) are shown at the bottom divided into those eruptions at latitudes less than and greater than 30° of latitude.

this approach for trend analysis of the 20 years of SAGE II measurements. A simple comparison of the volcanically quiescent periods in the SAGE II measurements, Figure 5.4, would preclude such a conclusion. Figure 5.4 suggests either a decline in background stratospheric aerosol or background was not reached at most latitudes prior to the eruption of Pinatubo.

Table 5.3 provides the parameters which were obtained from the non-linear least squares regression applied to the zonally-averaged SAGE II optical depths. Inspection of the fifth and sixth column of the table indicates that the long term trend in the background aerosol is not significantly different from zero. In contrast to the lidar and in situ data the decay rates following El Chichón are significantly different, about a factor of 2 less than the decay rates following Pinatubo. Is this a result of the missing data following El Chichón? To test this, the
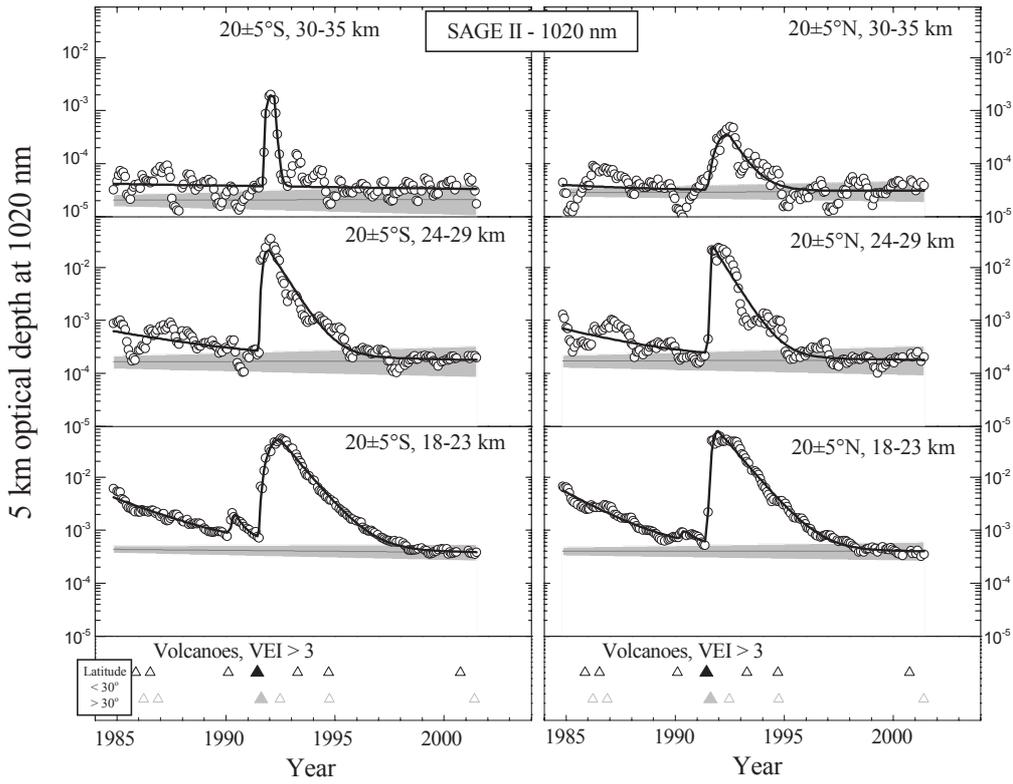
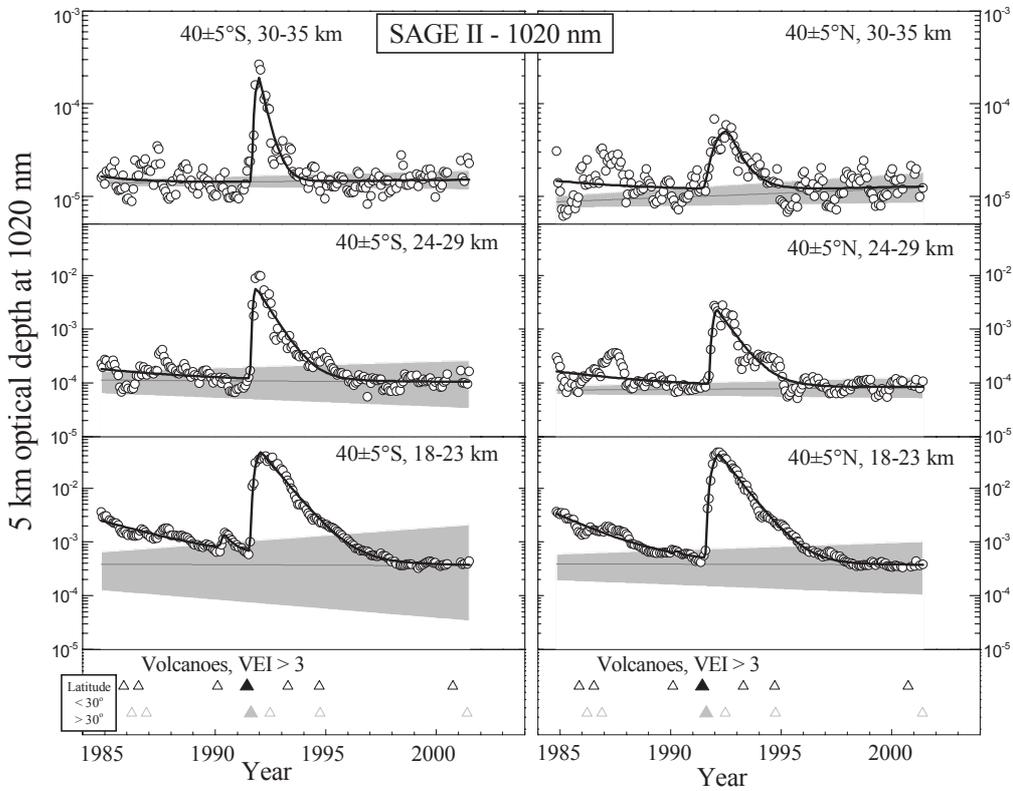**Figure 5.10. Same as Figure 5.9, except for latitudes of ± 20°.**

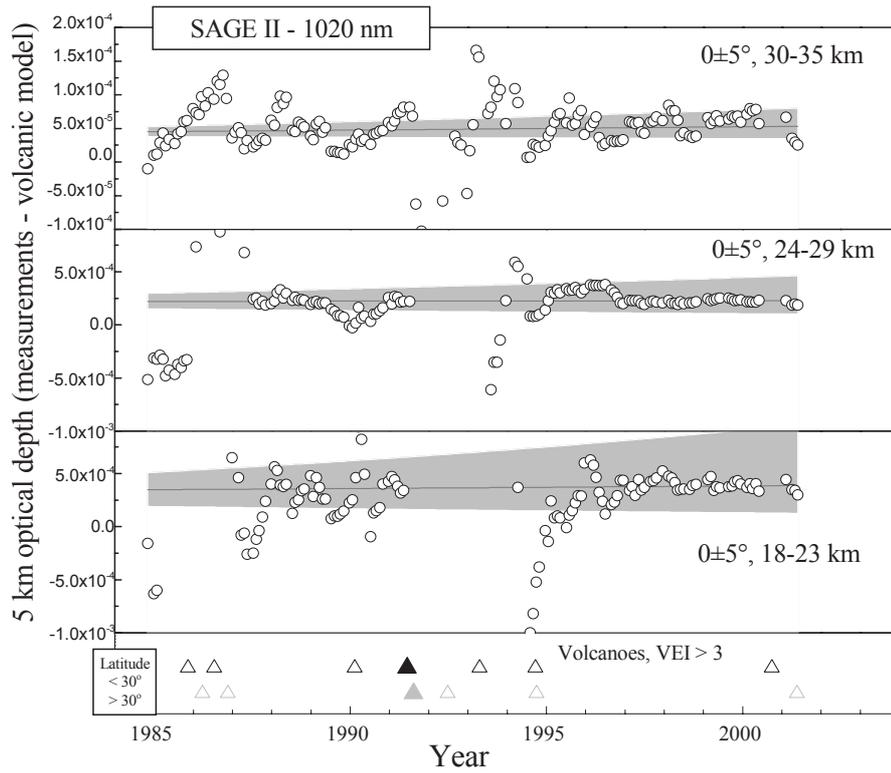**Figure 5.11. Same as Figure 5.9, except for latitudes of ± 40°.**

Figure 5.12. Same as Figure 5.9, except the data points are the measurements with the volcanic effect estimated from the model subtracted.
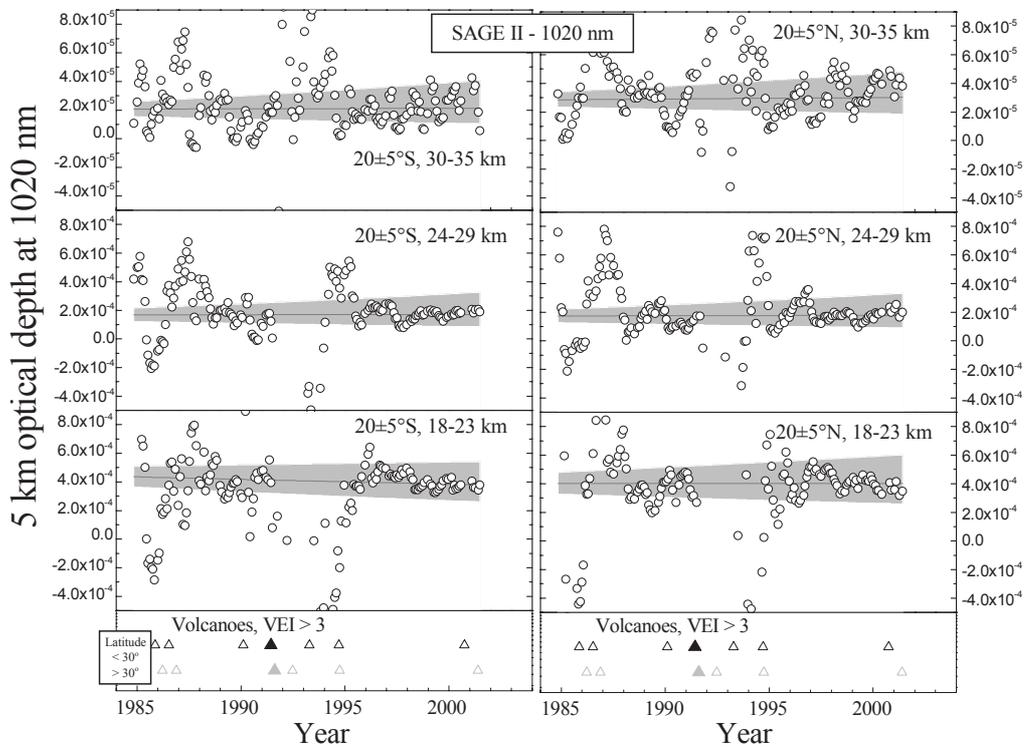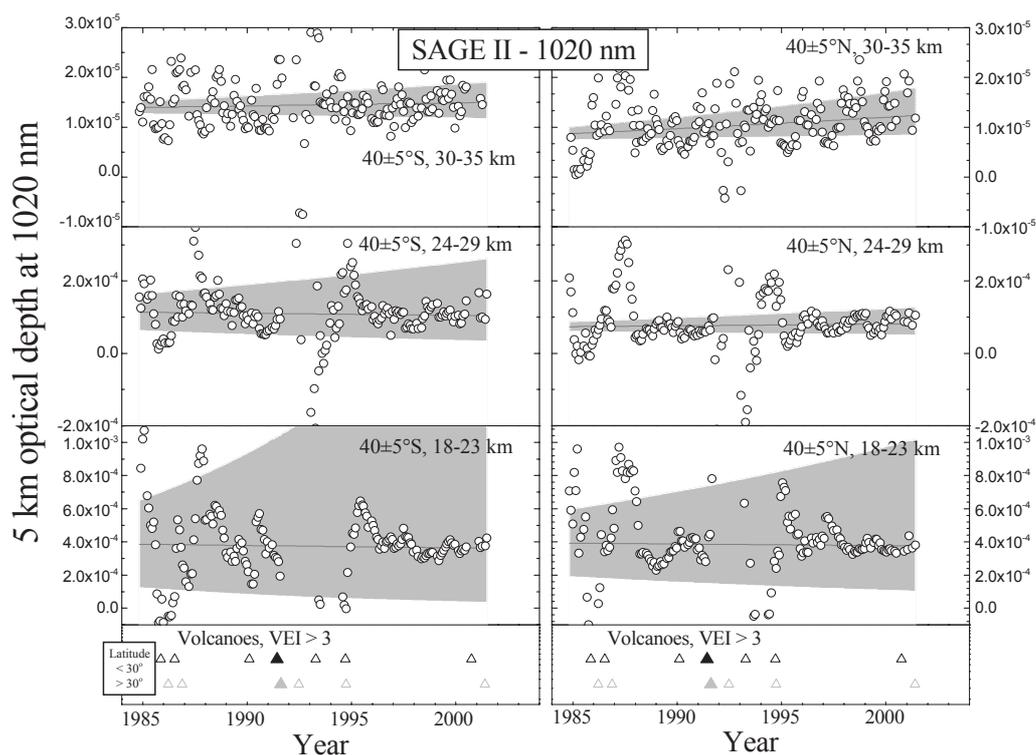

Figure 5.13. Same as Figure 5.10, except the data points are the measurements with the volcanic effect estimated from the model subtracted.

Figure 5.14. Same as Figure 5.11, except the data points are the measurements with the volcanic effect estimated from the model subtracted.

parametric model was rerun for the SAGE II 18-23 km optical depth at 40°N, but removing data for the two years following Pinatubo. The results did not change significantly. The estimated Pinatubo aerosol decay rate, and background aerosol change rate, changed by less than 1%, while confidence intervals increased by about 10 %.

Figure 5.15 provides the latitude distribution of the background decay term, β (yr^{-1}), with 95% confidence intervals for (1) SAGE II 1020 nm 5 km optical depths at three altitudes, (2) four lidar records and (3) in situ measurements at two sizes. All data records are consistent in providing estimates not significantly different from zero except for the Hampton lidar and Laramie 0.25 μm in situ measurements. As mentioned above, both of these data sets were highly perturbed by Mt. St. Helens, in comparison to other sites, and this perturbation created problems in establishing the baseline prior to El Chichón. Thus, while these two datasets suggest, at a minimum, no long term increase in background aerosol, they do not establish a long term decrease.

5.5   Discussion

The preceding analysis of background stratospheric aerosol suggests that there has been no long term trend in this quantity in the past 30 years. Thus the present long volcanically quiescent period, following Pinatubo, allows us to characterize rather completely stratospheric background aerosol, and provides a test bed for comparison of integral properties of

Table 5.3. Parameters used to model zonal, ± 5°, five kilometer optical depths at 1020 nm from SAGE II. Optical depth (× 10⁴) and exponential change (yr-1) are given for the baseline and the major impacts of El Chichón and Pinatubo along with their standard errors (σ). The 95% confidence intervals are given by parameter ± 2 σ.

Alt	Lat	Background				El Chichón				Pinatubo			
km	°	B	σ(B)	β	σ(β)	P	σ(P)	ν	σ(ν)	P	σ(P)	ν	σ(ν)
18-23	-50	3.00	0.15	0.0055	0.003	15.5	0.96	0.27	0.03	369	19.5	1.19	0.03
18-23	-40	3.86	2.32	-0.0039	0.037	21.4	2.12	0.31	0.05	460	22.0	1.15	0.03
18-23	-30	3.87	0.32	-0.0019	0.006	27.8	1.29	0.34	0.02	436	16.0	1.14	0.02
18-23	-20	4.36	0.37	-0.0083	0.006	37.9	1.64	0.40	0.02	512	18.3	1.14	0.02
18-23	-10	3.74	0.50	0.0014	0.009	60.6	3.09	0.44	0.02	1190	52.0	1.05	0.02
18-23	0	3.48	0.80	0.0064	0.016	93.5	7.17	0.53	0.03	1150	74.6	1.10	0.41
18-23	10	3.74	0.60	0.0043	0.011	82.5	5.37	0.56	0.03	1000	58.1	1.05	0.02
18-23	20	4.03	0.38	-0.0003	0.007	53.3	2.85	0.54	0.02	749	34.6	1.11	0.02
18-23	30	4.15	0.30	-0.0015	0.006	39.8	1.89	0.51	0.02	519	19.5	1.19	0.02
18-23	40	3.92	1.01	-0.0027	0.018	30.2	1.56	0.47	0.05	414	17.9	1.21	0.03
18-23	50	2.97	1.13	0.0082	0.025	21.7	1.42	0.41	0.06	287	16.2	1.18	0.04
24-29	-50	0.06	0.00	0.0009	0.009	0.1	0.00	0.00	0.01	2.3	0.4	2.97	0.27
24-29	-40	0.07	0.01	0.0002	0.009	0.1	0.01	0.00	0.01	1.8	0.3	2.75	0.35
24-29	-30	1.27	0.12	0.0008	0.009	1.6	0.30	0.23	0.06	88.0	11.4	1.49	0.10
24-29	-20	1.61	0.23	0.0028	0.011	4.9	0.60	0.24	0.03	235	30.3	1.34	0.07
24-29	-10	2.06	0.31	0.0008	0.012	10.9	0.91	0.25	0.02	484	47.1	1.33	0.05
24-29	0	2.22	0.37	0.0014	0.013	14.7	1.37	0.30	0.03	463	45.2	1.26	0.05
24-29	10	2.01	0.30	0.0043	0.012	11.3	1.14	0.32	0.03	339	37.5	1.36	0.06
24-29	20	1.73	0.24	0.0021	0.011	5.5	0.77	0.30	0.05	248	37.5	1.53	0.08
24-29	30	1.08	0.13	0.0029	0.011	2.1	0.37	0.27	0.06	72.6	10.2	1.44	0.10
24-29	40	0.74	0.07	0.0060	0.008	0.9	0.16	0.22	0.05	22.0	2.9	1.39	0.12
24-29	50	0.45	0.05	0.0043	0.010	0.5	0.06	0.07	0.02	10.1	1.4	1.35	0.14
30-35	-50	0.11	0.01	0.0000	0.005	0.0	0.02	0.56	1.04	1.7	0.2	2.66	0.27
30-35	-40	0.14	0.01	0.0044	0.005	0.0	0.02	0.44	0.39	1.8	0.3	2.68	0.33
30-35	-30	0.11	0.01	0.0005	0.011	0.1	0.01	0.01	0.01	5.0	0.9	12.9	2.98
30-35	-20	0.21	0.03	0.0017	0.013	0.2	0.03	0.03	0.02	19.6	5.6	11.9	2.12
30-35	-10	0.43	0.04	0.0065	0.009	0.4	0.14	0.46	0.18	10.1	1.9	1.62	0.20
30-35	0	0.45	0.04	0.0099	0.008	0.5	0.13	0.45	0.13	11.1	1.6	1.48	0.14
30-35	10	0.38	0.03	0.0054	0.008	0.3	0.08	0.29	0.10	5.2	0.6	1.50	0.20
30-35	20	0.29	0.03	0.0035	0.009	0.1	0.05	0.19	0.12	3.3	0.4	1.58	0.27
30-35	30	0.13	0.01	0.0199	0.009	0.1	0.02	0.15	0.06	1.4	0.2	1.62	0.32
30-35	40	0.09	0.01	0.0212	0.007	0.1	0.01	0.15	0.05	0.4	0.1	1.56	0.23
30-35	50	0.09	0.00	0.0065	0.005	0.0	0.01	0.22	0.36	0.3	0.0	1.69	0.24

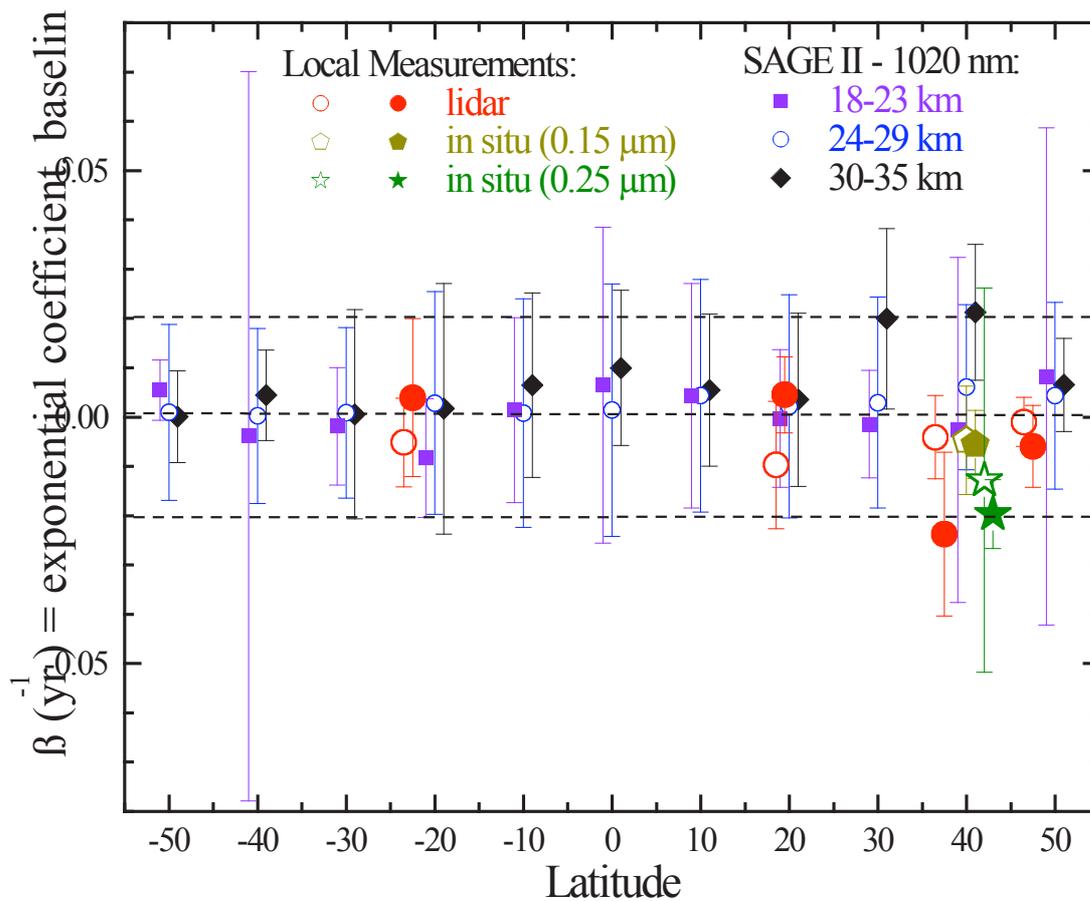**Figure 5.15. Exponential coefficient , β (yr^{-1}) ± 95% confidence interval, as a function of latitude for ± 5° zonal averages of 5 km optical depths at 1020 nm from SAGE II for three altitude intervals, for integrated backscatter from São José dos Campos, Mauna Loa, Hampton, and Garmisch, and for 15 - 30 km column integrals of aerosol concentration for particles with radius ≥ 0.15 and 0.25 μm. For the lidar and in situ data the open symbol represents β based on the analysis of quiescent periods, while the closed symbol represents β obtained from the parametric model. In all cases the values of**

stratospheric aerosol, e.g. aerosol surface area and mass, derived from different measurements. Here two such comparisons to address two questions related to background stratospheric aerosol are presented. How well do satellite measurements estimate aerosol surface area under conditions of low aerosol loading when median particle radii for surface area are well below the primary range of sensitivity for satellite extinction measurements at visible wavelengths? What is the global background stratospheric aerosol burden? Although these questions have been considered previously, there is no previous time in the modern aerosol measurement record when stratospheric aerosol have had such an opportunity to relax to a natural state unperturbed by volcanic activity.
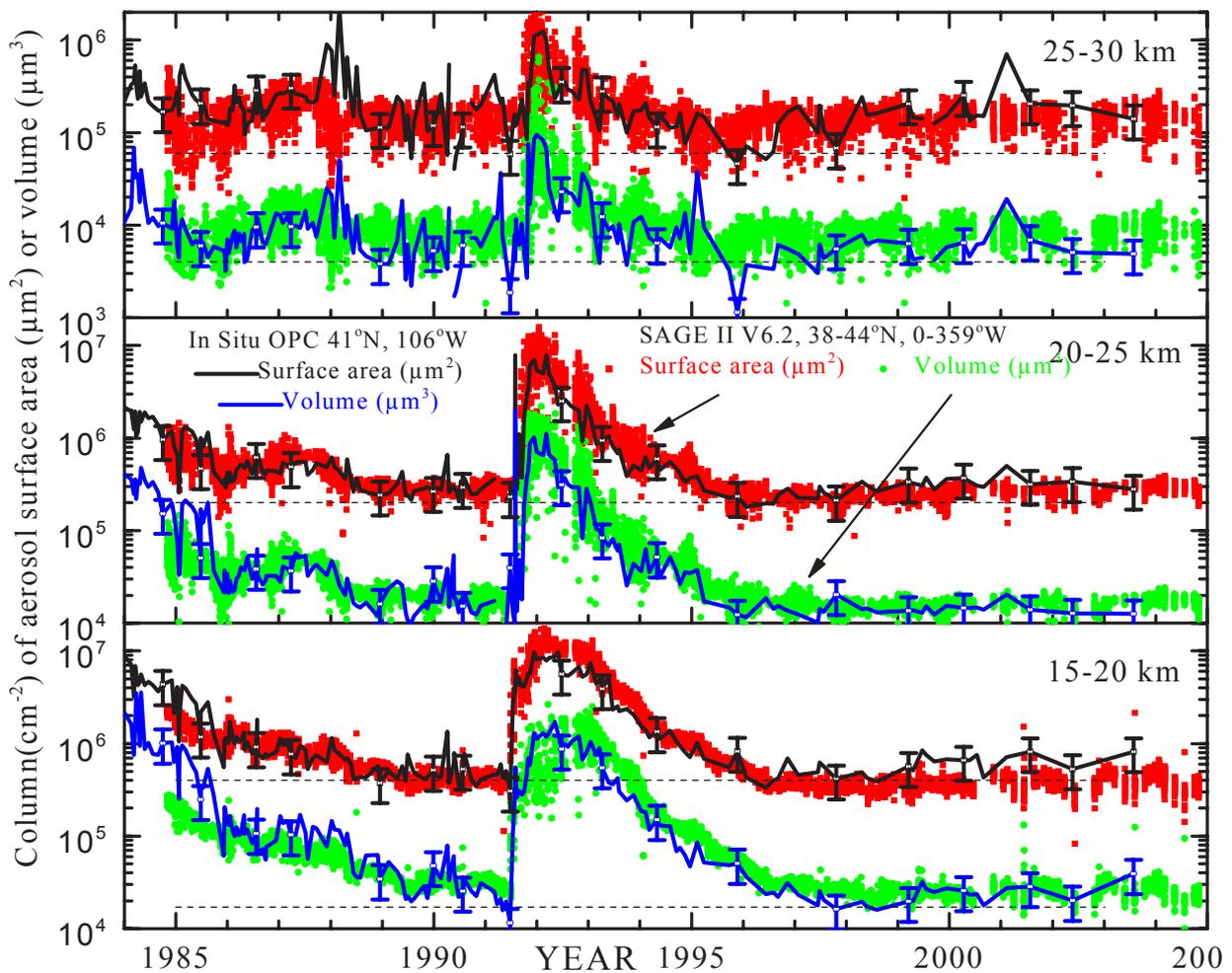
Figure 5.16. History of five kilometer column aerosol surface area and volume in the northern mid latitudes,1984-2004. The solid lines with intermittent error bars (±40%) are from lognormal size distributions fit to ~ 200 aerosol profiles from balloonborne in situ measurements above Laramie, Wyoming. The symbols are SAGE II V6.2 estimates of surface area and volume from the SAGE II data base for all measurements between 38 and 44°N with no restriction on longitude.

5.5.1 Aerosol surface area: Differences between satellite and in situ measurements

During periods of low stratospheric aerosol loading measurement precision generally decreases as the aerosol signal decreases. Satellite measurements and in situ measurements are perhaps the least impacted. There may, however, be an effect on the retrieval of aerosol surface area from satellite measurements at visible wavelengths [Steele et al., 1999; Randall et al., 2001; Deshler et al. 2003]. Typically surface areas and volumes are calculated from visible wavelength extinction measurements using principal component analysis [Twomey, 1977; Thomason and Poole, 1993; Steele et al., 1999]. Figure 5.16 compares two of the longest records of stratospheric aerosol surface area and volume available [Deshler et al., 2003]. The SAGE II aerosol moments are from the SAGE II data base (V6.2). The SAGE II operational algorithm was described in Chapter 4 and relies heavily on the SAGE II measurements at 525 and 1020 nm. The SAGE II data in Figure 5.16 include all SAGE II measurements between 38 and 44°N. These aerosol moments are similar to moments obtained

by Steele et al. [1999] for high aerosol loading, but are higher than Steele et al. [1999] for background aerosol.

The agreement between the two data sets is well within measurement precision over the record as the stratospheric aerosol transitions from a volcanic to a background state. For this transition the relationship between in situ and satellite volume estimates remains roughly equivalent, with the in situ estimate at the lower range of the satellite estimate. For surface area the relationship between in situ and remote estimates changes, with in situ measurements moving from the lower range to the upper range of the satellite estimates in the transition from volcanic to background.

A physical explanation for the systematic change in the relationship of surface area estimates is offered in Figure 5.17. Differential surface area, volume, and extinction distributions are compared for measurements at two altitudes in 1993, under high aerosol loading, and at two altitudes in 1999, under low aerosol loading. At high aerosol loading there is good overlap between the three differential distributions, Figures 5.17a, b. The median radii of the three distributions, r_s, r_e, r_v, are nearly co-located, particularly at 18 km. At 23 km on 931115 $r_s < r_e$, but there is still excellent overlap of the distributions particularly in the dominant second mode. At low aerosol loading there are significant differences in the median radii and in the sizes covered by the different distributions, Figures 5.17c, d. In low aerosol loading cases, aerosol surface area is controlled by particles between 0.02 and 0.5 μm, $r_s \sim 0.1$ μm, and
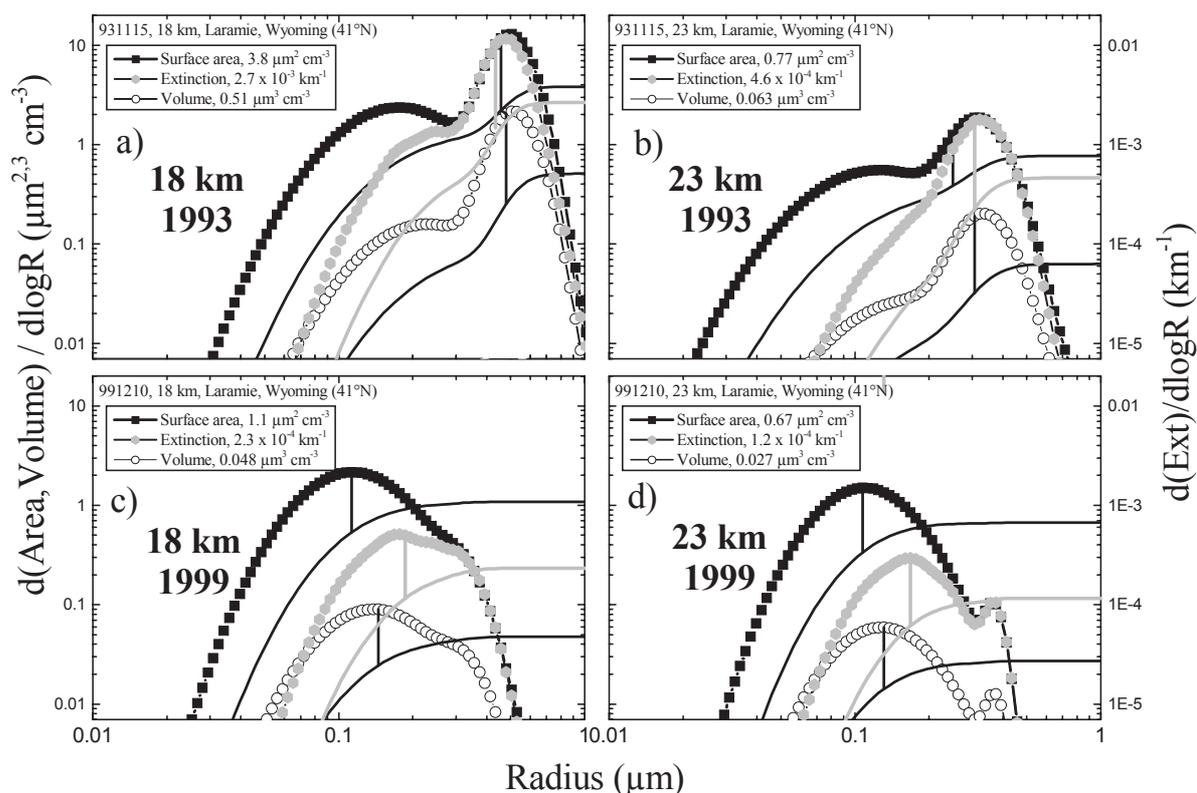

Figure 5.17. Differential (lines and symbols) and cumulative (lines) distributions of aerosol surface area, extinction, and volume at 525 nm for measurements above Laramie, Wyoming, at two altitudes 18 and 23 km for measurements 1.5 years after Pinatubo, 931115, and at low aerosol loading, 991210. The distributions are derived from in situ measurements of aerosol size distribution. The vertical line connecting the differential and cumulative distributions indicates the distribution median radius, i.e. 50% of the cumulative distribution moment is above and below this size. The values of the integrated distribution moments are shown in the legend.

~80% of the total surface area is contributed by particles < 0.15 μm. In contrast the extinction distribution is controlled by particles between 0.05 and 0.5 μm, $r_e \sim 0.2$ μm, and about 25% of the extinction signal is provided by particles less than 0.15 μm. There is less disparity between extinction and volume distributions. Although $r_v < r_e$, the size range spanned by these two distributions is quite similar in both high and low aerosol loading.

Figure 5.17 suggests that under low aerosol loading the use of extinction measurements to infer aerosol surface area may lead to a systematic underestimation, since aerosol surface area is controlled primarily by particles which contribute minimally to extinction. Accurate measurements of aerosol surface areas under clean stratospheric conditions, even from balloonborne in situ measurements, is also uncertain since the dominant mode of the distribution is captured by just a few measurements: condensation nuclei (CN, r > 0.01 μm), and aerosol > 0.15, 0.25 μm. The latter measurements only fix the tail of the distribution and are well above r_s. For the in situ measurements the size distribution of particles between 0.01 (CN) and r > 0.15 μm is calculated using unimodal lognormal distributions fit to measurements of the concentration of CN and particles > 0.15 μm. The standard method optimizes the fit to the number concentration measurements with size dependent weighting. A fitting method weighted by surface area produced results which were marginally different than the standard method. A comparison using ~450 measurements split between high and low aerosol loading indicated an increase of 12 ± 36% in surface area for surface area weighted fits to the data compared to no weighting. This result would increase the discrepancy between the in situ and satellite data shown in Figure 5.16; however, 12% is well within the ± 40% precision associated with the surface area estimates from the in situ measurements [Deshler et al., 2003].

More accurate measurements of surface area require size resolved concentration measurements between 0.01 and 0.1 μm. Present aircraft instruments are capable of this with size-resolved measurements for particles > 0.03 μm [Jonsson et al., 1995], but resolution of particle sizes below 0.15 μm from balloonborne platforms must await instruments now in the development stage. For a preliminary assessment of the difficulties a lack of size resolution below 0.15 μm presents for estimates of surface area from balloonborne in situ measurements, stratospheric aircraft measurements from the Focused Cavity Aerosol Spectrometer (FCAS) [Jonsson et al., 1995] were analyzed. FCAS measurements between 0.03 and 1.67 μm radius in 32 size bins were used to simulate measurements from OPCs sensitive to CN, r > 0.01 μm, and particles > 0.15 - 2.0 μm in 12 size bins. Bimodal lognormal distributions were then fit to the simulated OPC measurements and estimated aerosol surface areas were compared to surface areas calculated from the discrete size distributions measured by the FCAS. FCAS measurements from 23 September 1997 (20°N - 5°S, θ=380-500K) and 11 March 2000 (61-75°N, θ=400-470 K) were used. The lognormal fits to the simulated measurements reproduced the measured size distributions and surface areas reasonably well, Figure 5.18a; however, there was a systematic overestimation of the surface area by the simulated OPC measurements. Comparisons using ~250 measurements on each day indicated that fits to the simulated OPC data overestimated surface area by 7±15 % on 23 September 1997 and 26±22% on 11 March 2000. The primary source of error was in fitting distributions to the first mode which were too narrow, resulting in under/over estimates of surface area for particles smaller/larger than the median radii, Figure 5.18b. The overestimation at larger sizes generally overcompensates for under estimation at smaller sizes. For wider first mode distributions, Figure 5.18a, the observations were matched reasonably well and the estimated surface areas were close to the FCAS measurements. Distribution median radii were estimated
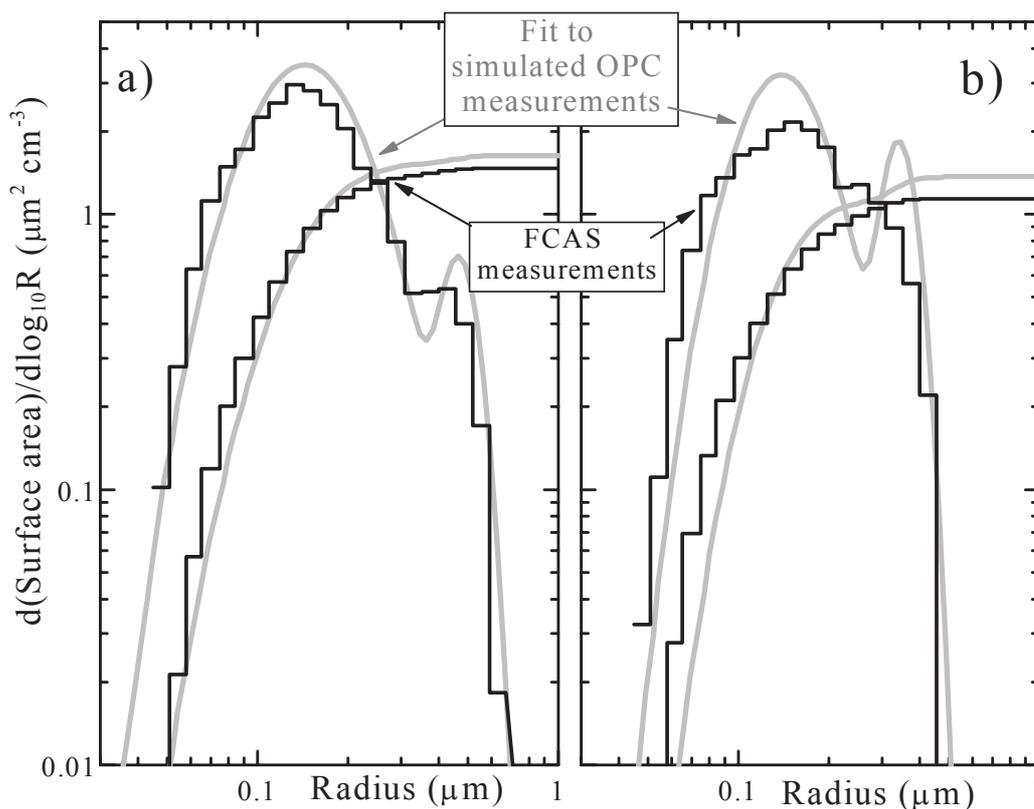
Figure 5.18. Differential and cumulative surface area distributions from discrete FCAS measurements and from bimodal lognormal distributions fit to simulated OPC measurements derived from the FCAS measurements. The two size distributions represent examples of a good fit, left panel, and a poor fit, right panel.

reasonably well even though the median radii of the first mode was always less than 0.1 μm, well below the first size resolved measurement by the OPC. Thus part of the discrepancy observed in Figure 5.16 may result from overestimates by the OPC; however, this does not fully account for the approximately factor of 2 difference in the worst cases.
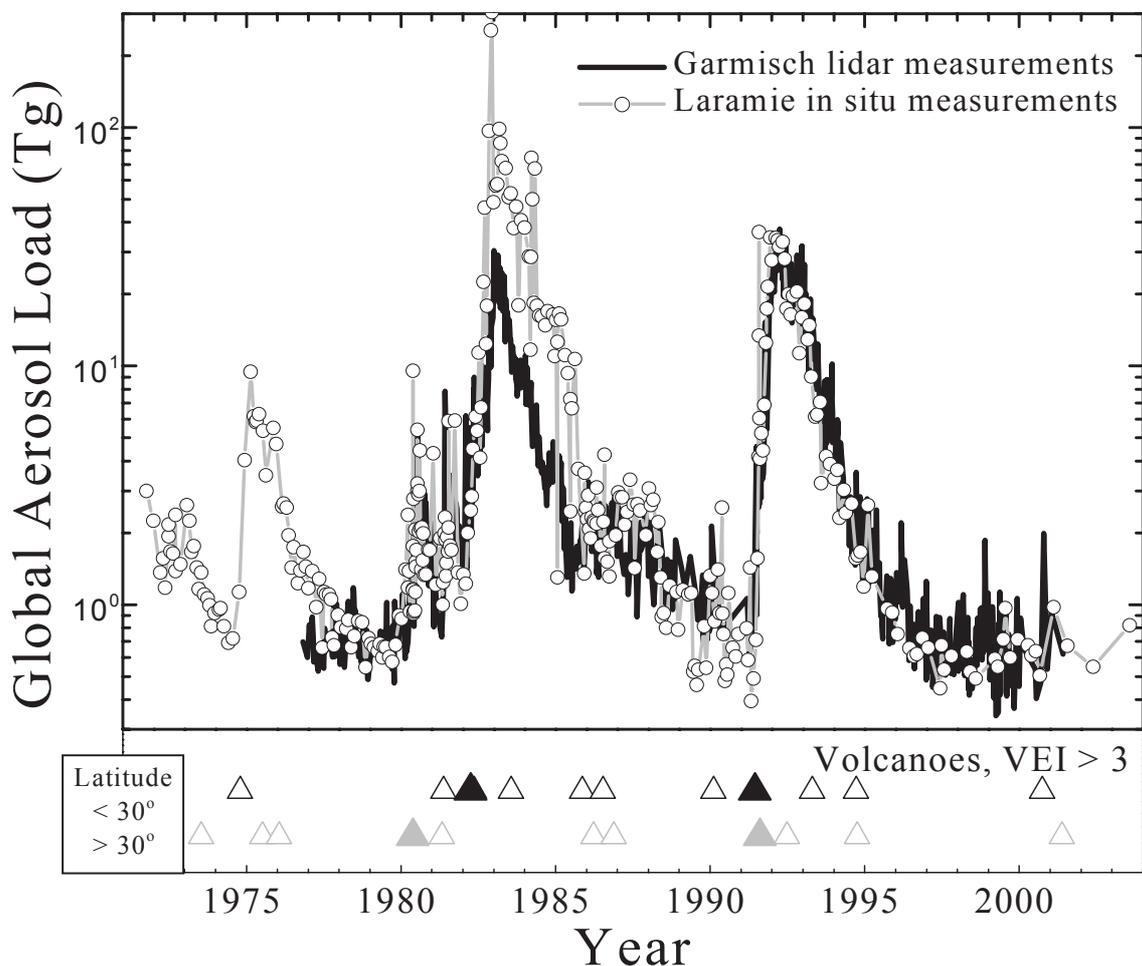
5.5.2 Estimates of global stratospheric aerosol burden during background conditions

The source of sulfur for non-volcanic stratospheric aerosol has been discussed since Crutzen's [1976] initial suggestion of OCS. Work in the mid 1990s [Chin and Davis, 1995] suggested that an additional source of sulfur may be required as known emission rates of OCS were insufficient to maintain the background stratospheric aerosol load observed. The measurements discussed here have been compared to the models of Timmrick [2001] and Weisenstein et al. [1997], which use OCS, SO_2 and transport of tropospheric sulfate aerosol into the stratosphere for sulfur sources. These models, if anything, overestimate the background stratospheric aerosol burden when model calculations are compared to aerosol concentrations at specific sizes (Figure 5.2) or integrated backscatter (Figure 5.3). To provide rough estimates of the mass loading which sulfur sources must provide during non-volcanic periods, two single measurement sites are extrapolated to estimate the global stratospheric aerosol load. Although such an extrapolation requires large assumptions, it is believed to provide better than an order of magnitude estimate. The estimates are tied to observations by

normalizing the estimates to 30 Tg of aerosol at the peak of Pinatubo aerosol loading [McCormick et al., 1995].

Extrapolations were made from estimates of integral columns of aerosol volume, from in situ measurements at Laramie, Figure 5.2 and Deshler et al. [2003], but using a 15-30 km column integral, and from aerosol mass inferred from Garmisch integrated backscatter, Figure 5.3 and Jäger [2005]. The integrated backscatter is converted to aerosol mass using Jäger and Deshler [2002, 2003] resulting in estimates provided by Jäger [2005]. Aerosol volumes are converted to aerosol mass using a density of 1.6 g cm^{-3}.

The stratospheric volume containing aerosol was estimated using a simple three cell model with integration limits defined as 18-36 km, 0-30°, 12-33 km, 30-60°, and 10-30 km, 60-90°.

Figure 5.19. **Estimates of stratospheric aerosol load based on an extrapolation from in situ profile measurements of aerosol size distribution above Laramie, Wyoming (41°N) and from integrated backscatter measurements above Garmisch (47°N). The in situ measurements use 15-30 km integrated aerosol volume, Figure 5.16, converted to column mass using an aerosol density of 1.6 g cm^{-3}. For backscatter the integrated backscatter columns are converted to mass using Jäger and Deshler [2002, 2003]. The profile measurements are then assumed to apply globally and thus integrated over the stratosphere, with the final result normalized to 30 Tg for Pinatubo. The time of volcanic eruptions with VEI ≥ 4 (open triangle) and 5 (closed triangle) are shown at the bottom divided into those eruptions at latitudes less than and greater than 30° of latitude.**

The very gross assumption is then made that the aerosol column measured at either Laramie or Garmisch can be used globally for background conditions. The calculations were then normalized to the Pinatubo aerosol load, which has been estimated at 30 Tg of aerosol [McCormick et al., 1995]. The normalization factor for both the in situ and lidar measurements was 0.65, which is surprisingly reasonable given the very large assumptions involved.

Using this simple model the aerosol load extrapolated from the Laramie and Garmisch measurements is shown in Figure 5.19. The usefulness of such a model can be seriously questioned, but it is heartening that the aerosol load shown in Figure 5.19 for Fuego agrees with previous estimates of 3-6 Tg, Table 5.1. The estimates for El Chichón from the in situ measurements are, however, factors of 4-5 too high. This may result from problems resulting from being unable to estimate aerosol concentrations for particles between 0.4 and 1.0 μm resulting from El Chichón compared to direct measurements in this size range following Pinatubo [Deshler et al., 2003]. The Garmisch lidar estimate, using the same model, also normalized to 30 Tg for Pinatubo, gives a maximum of approximately 20 Tg for El Chichón which is above the estimate given in Table 5.1, but closer than the in situ estimate of maximum loading. Based on this rough confirmation of such an extrapolation, the results for background stratospheric aerosol load are approximately 0.6±0.1 (0.7±0.2) Tg for the Laramie in situ (Garmisch lidar) measurements based on averages and population standard deviations for the 1997 - 2003 period. The uncertainties do not account for instrumental uncertainty or uncertainty in the global extrapolation of the measurements. When the in situ data are used to estimate aerosol mass, the elevated 0.25 μm particle concentrations observed in 1990, prior to the eruption of Pinatubo, are not apparent. This is in contrast to Figures 5.2 and 5.5. Instead the measurements in 1990 are similar to the post 1997 measurements.

5.6   Summary and Conclusions

Understanding the non-volcanic fraction of stratospheric aerosol has been one focus of stratospheric aerosol measurements since these measurements began over 40 years ago. Questions such as what are the source gases, how are they transported and transformed in the stratosphere, has there been an impact on natural background levels due to air traffic or other anthropogenic activities, and has the natural background aerosol changed over the course of measurements, have motivated measurements and analyses of background periods. Providing measurements to address these questions, however, has been difficult due to fairly active volcanism over the past 40 years, Table 5.1, with only the post Pinatubo period providing an interval allowing perhaps the first truly non-volcanic aerosol measurements since regular measurements began in the early 1970s. Thus this period provides our best opportunity to observe a stratosphere unperturbed by volcanic activity since long term stratospheric aerosol measurements began.

Junge et al. [1961] initiated stratospheric aerosol measurements in the late 1950s, which was at the end of a volcanically quiescent period. For this reason these measurements provided a baseline against which measurements in the 1970s and 1980s were compared. This provided the basis for early assessments of stratospheric aerosol which concluded that there had been an increase in the background aerosol. Now, with the benefit of minimal volcanism since Pinatubo, a definitive comparison with Junge's initial measurements, Figure 5.1, can be completed. From this comparison, and the stability of measurements following the decay of

Pinatubo volcanic aerosol, it is concluded that Junge's initial in situ measurements underestimated the size range or number concentration, or both, and thus the stratospheric aerosol measurements which can be reliably used to assess trends in the non-volcanic component of stratospheric aerosol began in the early 1970s. Earlier assessments of trends in non-volcanic stratospheric aerosol, which included Junge's initial measurements, 1959 - 1960, were probably premature. This interpretation is predicated on the assumption that the source gases for background stratospheric aerosol were relatively stagnant over this period.

During volcanically quiescent periods the sulfur for stratospheric aerosol arises from the transport of tropospheric OCS, SO_2, and sulfate aerosol into the stratosphere. If the fractional contributions of these source gases (35, 25, 40%) to stratospheric aerosol are coupled with trends in OCS [Montzka et al., 2004] and anthropogenic SO_2 [van Ardenne et al., 2001] a change in background stratospheric aerosol can be estimated for 1960-1990. These estimates indicate an increase of ~0.5% yr^{-1}, well below the earlier estimates of 5-9% yr^{-1} and even the more conservative estimate of 2% yr^{-1} indicated in Figure 5.1.

To provide an objective analysis of the stratospheric aerosol record since 1970 the statistical analysis of the six long term stratospheric aerosol records (1 in situ, 4 lidars, 1 satellite) were approached in two ways. First, measurements limited to the three volcanically quiescent periods were compared using standard techniques. Second, an empirical model was developed to remove the volcanic signal from the long term records and to investigate the "de-volcanized" measurements for trend. The data sets used for the analyses are: a) column integrals of in situ concentration measurements from Laramie, Wyoming, at two sizes, 0.15, 0.25 μm; b) integrated backscatter above the tropopause from Garmisch-Partenkirchen, Germany; Hampton, Virginia; Mauna Loa, Hawaii; and São José dos Campos, Brazil; and c) SAGE II extinction. The in situ measurements provide 2 data sets, 15 - 30 km column integrals of aerosol ≥ 0.15, 0.25 μm radius. The lidar records provide 4 data sets. The SAGE II measurements were separated into 33 data sets: zonal (±5°) averages of 5 km optical depths at 1020 nm for 18-23, 24-29, 30-35 km. These data are centered at latitudes of 0, ±10 … ±50°. SAGE data were included with the SAGE II data for some trial cases, but this did not change conclusions based just on the SAGE II data. The possibility of augmenting these data with SAM measurements was investigated, but there was no latitudinal overlap since the SAGE II data were limited to latitudes ≤ 50° to avoid polar stratospheric clouds. Consideration of SAM II data alone was deemed not helpful once the records were limited to non polar stratospheric cloud periods.

Simple inspection of the long term records suggests that: a) There have been fewer small volcanic eruptions following Pinatubo than during the two previous volcanically quiescent periods. b) The pre-Pinatubo period is elevated compared to the post Pinatubo and pre-El Chichón period. c) The post Pinatubo period and pre-El Chichón period thus control any conclusions regarding long term changes. d) Volcanic aerosol from Pinatubo disappeared from the long term measurement records between 4.5 and 7.5 years following the eruption, dependent on latitude and measurement platform. e) The post Pinatubo period represents our best opportunity to observe a stratosphere unperturbed directly by volcanic activity. f) The current low aerosol levels are believed due to the long period of limited volcanic input. g) Stratospheric aerosol are not expected to fall significantly below current levels, although longer-term variations cannot be ruled out.

Comparison of measurements within the 3 volcanically quiescent periods indicates that only the 1 in situ and 4 lidar records capture the three volcanically quiescent periods, pre El

Chichón, pre Pinatubo and post Pinatubo. SAGE II only captures pre and post Pinatubo and the pre-Pinatubo SAGE II record is not convincingly at background. Investigation of the 5 longer records suggests that the first two periods may also not have reached background, particularly prior to Pinatubo. In 3 of the 4 lidar records (Garmisch, Hampton, São José), and in the 0.25 μm in situ record 15-30 km, the pre-Pinatubo period is elevated compared to the other periods. Simple linear regression over the three periods is controlled by the end points, pre El Chichón, post Pinatubo and indicates either no change (Garmisch, Hampton, São José dos Campos, Laramie-0.15 μm) or a slight decrease in stratospheric aerosol (Mauna Loa, Laramie-0.25 μm). Problems with a simple linear regression arise due to irregular temporal data and the high degree of autocorrelation. Including autocorrelation in the estimates decreases confidence in the estimates (increases standard errors), but does not change the conclusion that the majority of data indicate no trend in background stratospheric aerosol, 1970 - 2005. Two data sets, Mauna Loa and Laramie 0.25 μm, suggest slight negative trends of -1 ± 1.0% yr^{-1} and -1 ± 4% yr^{-1}, respectively. The results for Mauna Loa are borderline statistically significant when autocorrelation effects are considered. This analysis is dependent on the assumption that stratospheric aerosol in the short 1-2 year period prior to Mt. St. Helens in 1980 was at background.

A time and volcano dependent empirical model was fit to the long term aerosol records to "de-volcanize" the data and thus analyze the entire data set for trend. Working in log space was required to treat errors during cases of high and low aerosol load equally. The empirical model also included a parameter to capture trends in the background aerosol. A standard squared-error residual minimization technique was employed to estimate the optimum parameters for the model for each measurement and each site. This included 4 lidar data sets, 2 in situ data sets (two aerosol sizes) and 33 SAGE II data sets (optical depths at 1020 nm at three altitude and eleven latitude intervals). These analyses allowed for first order autocorrelation and used a one-dimensional spatial representation to account for the temporally disparate sampling intervals. As with the simpler comparison of background periods the autocorrelation increases the standard errors of the trends but does not change the magnitude. For 31 of 33 SAGE II data sets, 3 of 4 lidar records, and in situ measurements at 0.15 μm the analyses suggest no long term trend in stratospheric aerosol. For one lidar site (Hampton) and in situ measurements at 0.25 μm, the results suggest a weak negative trend, on the order of -2 ± 0.5% yr^{-1}. Both these estimates suffer from difficulties introduced by Mt. St. Helens, and a comparison of the model with the data suggests problems in representing properly the measurements prior to El Chichón. In contrast to these two estimates of a negative trend, two SAGE II data sets (30-35 km, 30° and 40°N) suggest a positive trend of the same magnitude, 2% yr^{-1}.

The overall conclusion from both the simple analysis of quiescent periods and the empirical model fit to the measurements is that background stratospheric aerosol has not displayed a long term trend over the period 1970 - 2005. This conclusion is supported by 94% of the satellite data analyzed, 75% of the lidar data, and 50% of the in situ data. The conclusion from the remaining data is not compelling. In addition to this result from statistical analyses, the long volcanically quiescent period following Pinatubo allows each record to be inspected for trend over a period of 5 to 8 years, and all are consistent in showing no significant change over this latter period.

The statistical analyses were completed on altitude/latitude integrals of the measurements, precluding establishing, or ruling out, long term changes in microphysical properties of background stratospheric aerosol. The focus on integral properties, an inherent limitation of

this investigation, is dictated by the fact that all but the in situ instruments make measurements on ensembles of particles and thus inherently integrate over the size distribution. Thus the in situ record was also integrated to provide a relatively homogenous data set for comparison with the other long term records. Some information concerning the long term tendency of aerosol size distributions is available by comparing altitude integrals of the two sizes, r > 0.15, 0.25 µm, measured. The simple comparison here indicates no change in the concentration of particles > 0.15 µm radius with a slight decrease for particles > 0.25 µm. This difference is not enough to be apparent in size distribution integrals, e.g. surface area or volume.

Background aerosol present special challenges for inverting surface area from optical extinction measurements. In background conditions median radii of aerosol size distributions are on the order of 0.07 µm. In these cases extinction at optical wavelengths is determined by less than 50% of the particles which determine surface area. This can lead to underestimates of aerosol surface area during background conditions. The background global stratospheric aerosol load was estimated to be 0.65 ± 0.2 Tg based on extrapolating in situ aerosol measurements at Laramie, and lidar measurements at Garmisch, between 1997 and 2003, to encompass the global stratosphere. The uncertainty quoted is the standard deviation of the estimates over the period 1997-2003.